Myonuclear alterations associated with exercise are independent of age in humans

[1,2,3]Battey, E., [2]Ross, J.A, [2]Hoang, A., [4]Wilson, D.G.S., [1]Han, Y., [1]Levy, Y., [1]Pollock, R.D., [1,5]Kalakoutis, M., [6]Pugh, J.N., [6]Close, G.L., [1]Ellison-Hughes, G. M., [1]Lazarus, N.R., [5]Iskratsch, T., [1]Harridge, S.D.R., [1,7,$] Ochala, J., & [2,$] Stroud, M.J.

[1]Centre for Human & Applied Physiological Sciences, Faculty of Life Sciences & Medicine, King's College London, London, UK

[2]British Heart Foundation Centre of Research Excellence, School of Cardiovascular Medicine and Sciences, King's College London, London, UK

[3]Novo Nordisk Foundation Center for Basic Metabolic Research, University of Copenhagen, Copenhagen, Denmark

[4]School of Engineering and Materials Science, Queen Mary University of London, London, UK

[5]Randall Centre for Cell and Molecular Biophysics, Faculty of Life Sciences & Medicine, King's College London, London, UK

[6]School of Sport and Exercise Sciences, Tom Reilly Building, Byrom Street, Liverpool John Moores University, Liverpool, UK

[7]Department of Biomedical Sciences, Faculty of Health and Medical Sciences, University of Copenhagen, Copenhagen, Denmark

[$] co-corresponding authors

Keywords: exercise, ageing, nuclei, nuclear shape, nuclear lamina

Key points

- The nucleus plays an active role in translating forces into biochemical signals
- Myonuclear aberrations in a group of muscular dystrophies called laminopathies suggest that the shape and mechanical properties of myonuclei are important for maintaining muscle function.
- Here, we present striking differences in myonuclear shape and mechanics associated with exercise, in both young and old humans.
- Myonuclei from trained individuals were more spherical, less deformable, and contained a thicker nuclear lamina than untrained individuals.
- We conclude that exercise is associated with age-independent myonuclear remodelling, which may help to maintain muscle function throughout the lifespan.

Abstract

Age-related decline in skeletal muscle structure and function can be mitigated by regular exercise. However, the precise mechanisms that govern this are not fully understood. The nucleus plays an active role in translating forces into biochemical signals (mechanotransduction), with nuclear lamina protein Lamin A regulating nuclear shape, nuclear mechanics, and ultimately gene expression. Defective Lamin A expression causes muscle pathologies and premature ageing syndromes, but the roles of nuclear structure and function in physiological ageing and in exercise adaptations remain obscure. Here, we isolated single muscle fibres and carried out detailed morphological and functional analyses on myonuclei from young and older exercise-trained individuals. Strikingly, myonuclei from trained individuals were more spherical, less deformable, and contained a thicker nuclear lamina than untrained individuals. Complementary to this, exercise resulted in increased levels of Lamin A and increased myonuclear stiffness in mice. We conclude that exercise is associated with myonuclear remodelling, independently of age, which may contribute to the preservative effects of exercise on muscle function throughout the lifespan.

Introduction

Human lifespan has increased substantially over the past half-century and this trend is projected to continue (UN, 2022). However, this has not been accompanied by an equivalent extension of the healthspan in old age; instead, morbidity has been extended, and independence and quality of life attenuated (Brown, 2015). Thus, a 'managed compression of morbidity' is essential to address social and economic issues associated with an extended lifespan (Brown, 2015). A contributing factor to morbidity is the decline in skeletal muscle structure and function associated with ageing. Muscle contractions produce force, allowing us to carry out whole-body movements such as walking, stair-climbing or rising from a chair – movements essential for independence and quality of life. The ageing process, however, is compounded by the physically inactive status of individuals in a technologically advanced society (Guthold *et al.*, 2018; Nikitara *et al.*, 2021). Furthermore, physical inactivity can accelerate the decline in physiological function that inevitably occurs during later years of life (Lazarus & Harridge, 2017; Shur *et al.*, 2021).

Skeletal muscle structure and function can be better maintained in old age by exercise, but the mechanisms behind this remain poorly understood (Wroblewski *et al.*, 2011; Pollock *et al.*, 2015; Lazarus *et al.*, 2019). An area of research which is understudied is how exercise and ageing influence the ability of skeletal muscle to translate force into biochemical signals (mechanotransduction) at the subcellular level. This is pertinent given the contractile nature of muscle and the opposing effects of exercise and inactivity on the frequency and intensity of muscle contractions. Emerging data suggest that the nucleus is a critical mechanosensor that orchestrates cell structure, function, and adaptive responses (Kirby & Lammerding, 2018). Indeed, the shape and mechanical properties of nuclei appear to regulate gene expression by altering genome organisation and ultimately influencing broader transcriptional profiles (Tajik *et al.*, 2016; Kirby & Lammerding, 2018; Piccus & Brayson, 2020; Kalukula *et al.*, 2022). Additionally, altered nuclear shape and nuclear envelope stretching can expand nuclear pore complexes and ion channels, facilitating translocation of mechanosensitive transcription factors Yes-associated protein/Transcriptional coactivator with PDZ-binding motif (Yap/Taz) and myocardin-related transcription factor (MRTF-A) or ions such as Ca^{2+}, respectively, altering gene expression and signalling (Kirby & Lammerding, 2018; Maurer & Lammerding, 2019; Ross & Stroud, 2021; Shen *et al.*, 2022).

Abnormal nuclear structure and responses to forces are hallmarks of numerous diseases that result in skeletal muscle weakness and premature ageing, commonly caused by mutations in nuclear envelope and associated proteins (Goldman *et al.*, 2004; Ross *et al.*, 2019; Battey *et al.*, 2020; Earle *et al.*, 2020; Kalukula *et al.*, 2022). Such proteins physically link the nucleus

87 to the cytoskeleton, providing a nexus for mechanotransduction (Crisp *et al.*, 2006; Banerjee
88 *et al.*, 2014; Kirby & Lammerding, 2018; Ross & Stroud, 2021). The nuclear lamina, which
89 lines the inner nuclear membrane and comprises Lamins A/C, B1 and B2, tethers chromatin
90 to the nuclear periphery, associates with nuclear pore complexes, and connects the
91 nucleoskeleton to the cytoskeleton via Linker of Nucleoskeleton and Cytoskeleton (LINC)
92 complex (Osmanagic-Myers *et al.*, 2015; Stroud *et al.*, 2017; Stroud, 2018; Owens *et al.*,
93 2021). Within this prominent location, the nuclear lamina is critically positioned to sense
94 cytoskeletal forces to regulate gene expression, biochemical signalling and overall cell
95 function and adaptation (Cho *et al.*, 2017; Maurer & Lammerding, 2019).

96 Importantly, various diseases caused by mutations in genes encoding nuclear lamina proteins
97 (termed laminopathies) primarily affect mechanically active muscle tissue and result in
98 aberrant nuclear shape, structural integrity and mechanotransduction (Janin *et al.*, 2017; Earle
99 *et al.*, 2020; Shin & Worman, 2021). One such laminopathy is Hutchinson-Gilford Progerin
100 (HGPS) syndrome, a premature ageing syndrome caused by a mutation in the gene encoding
101 Lamin A/C (Goldman *et al.*, 2004; Merideth *et al.*, 2008). Defective Lamin A/C expression also
102 results in muscular dystrophy characterised by muscle weakness (such as autosomal
103 dominant Emery-Dreifuss muscular dystrophy, limb-girdle muscular dystrophy type1B, and
104 *Lmna*-congenital muscular dystrophy) (Bonne *et al.*, 1999; Maggi *et al.*, 2016). Thus,
105 myonuclear shape, nuclear envelope proteins, and nuclear mechanics are dysregulated in
106 muscle pathologies and premature ageing syndromes and may have important roles in age-
107 related muscle dysfunction.

108 Lamin A/C has been shown to be required for normal nuclear mechanics in myotubes and for
109 cardiac and skeletal muscle overload hypertrophy responses in mice (Cupesi *et al.*, 2010;
110 Earle *et al.*, 2020; Owens *et al.*, 2021). Indeed, a congenital mutation in Lamin A/C causing
111 muscular dystrophy resulted in altered nuclear mechanics, attenuated hypertrophy and force
112 capacity in response to functional overload in mouse skeletal muscle (Owens *et al.*, 2021). In
113 cardiac tissue, in response to pressure overload, haploinsufficient Lamin A/C mice
114 demonstrated reduced ventricular mass and myocyte size and impaired mechanotransduction
115 (Gerhart-Hines *et al.*, 2007; Little *et al.*, 2010; Gurd, 2011). Collectively, these studies hint at
116 a potential Lamin A/C-dependent mechanosensitive signalling cascade in regulating both
117 muscle hypertrophy and oxidative exercise adaptations.

118 Despite the large amount of evidence suggesting the importance of nuclear shape, mechanics
119 and lamina in premature ageing and muscle pathologies, their roles in normal ageing and
120 exercise are poorly understood (Gerhart-Hines *et al.*, 2007; Little *et al.*, 2010; Cupesi *et al.*,
121 2010; Gurd, 2011; Earle *et al.*, 2020; Owens *et al.*, 2021). To this end, we investigated whether

ageing and exercise affected structure and function of skeletal muscle nuclei. Single muscle fibres from young and older trained and untrained individuals were isolated and myonuclear structure and function analysed. Detailed 2D and 3D morphological analyses of myonuclei revealed striking nuclear shape differences in trained individuals compared to untrained individuals, regardless of age. Additionally, myonuclei from trained individuals had increased nuclear lamina deposition and were less deformable compared to untrained counterparts. Consistently, skeletal muscle from trained mice had increased levels of Lamin A and increased nuclear stiffness. Our data suggest for the first time in humans that exercise is associated with differences in myonuclear shape and mechanics, that likely mitigate the deleterious effects of inactive ageing.

Methods

Ethical approval

Prior to participation, written informed consent was obtained from all subjects. Procedures were approved by the Fulham Research Ethics Committee in London (12/LO/0457), Westminster Ethics Committee in London (12/LO/0457) or Liverpool John Moores ethics committee (H17SPS012) and conformed to the standards set by the Declaration of Helsinki. All human tissues were collected, stored, and analysed in accordance with the Human Tissue Act. Procedures were performed in accordance with the Guidance on the Operation of the Animals (Scientific Procedures) Act, 1986 (UK Home Office); King's College London License number: X24D82DFF, ethics code: PDB33C80B.

Participant characteristics and ethics

Four mixed gender groups were recruited to participate in the current study (n = 6 per group). These groups were: younger untrained healthy (YU) (33 ± 9.5 years), younger trained marathon runners (YT) (32 ± 5.4 years), older untrained individuals (OU) (79 ± 11.3 years), and older highly trained cyclists (OT) (75.5 ± 3.2 years) (Table 1). The YU group was considered healthy, but not necessarily sedentary, as two of the participants had been participating in low-level recreational sport activities (<2 sessions/week) at the time of the study. Thus, the young cohort consisted of low-level physically active and sedentary individuals. Participants were considered healthy if they met the criteria outlined by Greig et al. (Greig *et al.*, 1994). The exclusion criteria from a healthy classification were smoking or consuming alcohol excessively, known hypertension or other cardiovascular, musculoskeletal, or neurological conditions, or if they were on any medication (acute or chronic). The YT group consisted of trained marathon runners ($\dot{V}O2$ peak 56.7 ± 6.6 ml.kg.min^{-1}, mean ± SD). In the YT group, the fastest running times (mean ± SD) in the previous 18 months over marathon, half marathon and 5 km distances were 204.5 ± 14.2 min, 88.5 ± 3.3 min, and 19.8 ± 1.3 min, respectively. The OU group, used as a model for muscle disuse in old age, was a previously characterised cohort, who underwent dynamic hip screw insertion surgery. The patients completed a basic physical health questionnaire and were considered eligible if they did not suffer from neuromuscular disease, although some had underlying health conditions (Table 1). The OT group consisted of previously characterised individuals (Pollock *et al.*, 2015) who were amateur master endurance cyclists. Master cyclists were included if they were able to cycle 100 km in under 6.5 hours (males) or 60 km in under 5.5 hours (females). Participants must have had completed this distance within the specified time on two occasions in the three weeks prior to the date of participation in the study.

167 **Table 1. Participant characteristics**

Group	Age	Sex	Height (cm)	Weight (kg)	BMI	Comment	Drug intake
Younger untrained	25	F	164	55	20.4		
	27	M	184	80	23.6		
	22	M	178	75	23.7		
	42	F	172	73	24.7		
	38	F	158	48	19.2		
	44	F	166	52	18.9		
Young marathon runners (younger trained)	35	M	182	71	21.4		
	32	M	176	67	21.6		
	32	F	170	64	22.1		
	22	M	190	70	19.4		
	38	M	170	68	23.5		
	34	F	160	55	21.5		
Older untrained	59	M	164	53	19.7	Osteoporosis	Perindopril, Amlodipine, Etidronate, Adcal
	91	F				Osteoporosis, Diverticulitis - Hartmann's bowel operation	Furosemide, Paracetamol, Colecalciferol, Docusate
	77	M				Osteoporosis	Paracetamol, Tramadol, omeprazol, renetadine, mirapixin, procloperizone
	82	F	152	57	24.7	Osteoporosis, Hypertension, Rheumatoid arthritis, type 2 diabetes	Metformin, denusomab, levothyroxine, allopurinol
	88	F	156	64	26.3	Osteoporosis, Breast cancer, left mastectomy in remission	Levothroxine, atenolol
	77	F		61		Osteoporosis, Rheumatoid arthritis	Sulfasalazine
Master cyclists (older trained)	71	M	180	83	25.7		
	76	F	157	58	23.4		
	79	F	159	53	21.1		
	75	M	172	62	20.8		
	73	M	170	70	24.0		
	79	F					

168 Obtaining and processing skeletal muscle samples and isolating single muscle
169 fibres

170 Vastus lateralis samples were obtained as previously described (Pollock *et al.*, 2018).
171 Approximately 60mg of the biopsy sample was then placed in relaxing solution (77.63 mM
172 KCL, 10 mM imidazole, 2 mM $MgCl_2$, 2 mM EGTA, 4.05 mM ATP in distilled water, pH 7.0) in
173 a petri dish on ice. Following excision, muscle samples (submerged in relaxing solution in a
174 petri dish) were divided into bundles of approximately 100 muscle fibres using forceps under
175 a stereo microscope (Zeiss, Stemi 2000-C) with a separate light source (Zeiss Stereo CL 1500
176 ECO). The ends of the bundles were then tied onto glass capillary tubes using surgical silk
177 (LOOK SP102) and stretched to approximately 110% of the original length. These bundles
178 were subsequently placed into 1.5 ml Eppendorf tubes, containing skinning solution (relaxing
179 solution with 50% (v/v) glycerol), at 4°C for 48 h to permeabilise the muscle fibres by disrupting
180 the lipid bilayer of the sarcolemma, leaving myofilaments, intermediate filaments, and nuclear
181 envelope intact (Konigsberg *et al.*, 1975; Wood *et al.*, 1975; Frontera & Larsson, 1997;
182 Stienen, 2000). Samples were then treated in ascending gradients of sucrose dissolved in
183 relaxing solution (0.5 M, 1 M, 1.5 M, 2 M) for 30 minutes to prevent cryodamage (Frontera &
184 Larsson, 1997). In a petri dish containing 2 M sucrose, fibres were then removed from the
185 glass capillary tubes before being placed in cryovials and snap-frozen in liquid nitrogen.

186 For immunofluorescence and nuclear mechanics experiments, muscle fibre bundles were
187 placed in descending concentrations of sucrose dissolved in relaxing solution, for 30 minutes
188 in each solution (2 M, 1.5 M, 1 M, 0.5 M, 0 M). Samples were transferred to skinning solution
189 at -20℃ until the day of an experiment. To isolate single muscle fibres, muscle bundles were
190 placed in skinning solution in a petri dish on an ice block. One end of the muscle bundle was
191 held using extra fine forceps, whilst single fibres were pulled from the end of the bundle. During
192 this process, care was taken to restrict contact to the ends of fibres as much as possible to
193 avoid damage. To normalise muscle fibre tension and orientation, muscle fibres were mounted
194 on half-split grid for transmission electron microscopy (TEM) glued to a coverslip (Ross *et al.*,
195 2017; Levy *et al.*, 2018). Fibres were then immunostained and imaged or analysed by a
196 nanoindenter to assess nuclear mechanics.

197 Immunostaining, imaging, and analysis of single muscle fibres

198 The first steps of each staining protocol were fixing in 4% PFA for 15 min and permeabilising
199 in 0.2% triton for 10 min. When primary antibodies were used, fibres were blocked using 10%
200 goat serum (Sigma-Aldrich, G9023) in PBS for 1 hour at room temperature before incubation
201 in primary antibody solution overnight at 4℃. Muscle fibres were then incubated in a solution
202 containing direct stains and secondary antibodies for 1 h (see list of primary and secondary in

203 Table 2). Finally, fibres were mounted in Fluoromount-G® or DAKO mounting medium.
204 Between each step of staining protocols, fibres were washed four times in PBS.

205 For two-dimensional analysis of myonuclear shape, single plane or z-stack images (1 μm Z
206 increments) were acquired using a 40x air objective and a Zeiss Axiovert 200 microscope
207 system. Two-dimensional myonuclear shape parameters (nuclear area and aspect ratio) were
208 quantified using Fiji software, as previously described (Schindelin *et al.*, 2012; Battey *et al.*,
209 2022). Single plane or maximum intensity projection images were processed with a rolling ball
210 background subtraction (150 pixels), gaussian blur filter (2 pixels radius) and despeckle
211 function before thresholding the DAPI signal (initially with 'Otsu dark' setting then adjusting as
212 necessary). Laterally located nuclei (i.e. positioned around the sides of muscle fibres) were
213 excluded from analysis as nuclei in this position are orientated perpendicular, rather than
214 facing the objective lens. Sarcomere length was quantified by measuring the distance between
215 ten sarcomeres using the segmented line tool in Fiji and dividing this value by ten.

216 For three-dimensional analysis of myonuclear shape and Lamin A organisation, Z-stack
217 images (0.2 μm Z increments) were acquired using a 60x oil objective and a Nikon spinning
218 disk confocal microscope system. To quantify three-dimensional shape parameters
219 (sphericity; skeletal length/diameter, referred to as 3D aspect ratio), the DAPI signal was
220 thresholded and analysed using Volocity software (Perkin Elmer). Skeletal length is the
221 maximum length of the object, which is eroded evenly from its border inwards until it consists
222 of a one-voxel thick, skeletal representation along its entire length. Skeletal diameter is the
223 diameter of a cylinder if it had a length equal to the skeletal length of the object and a volume
224 equal to the object's measured volume (from Volocity User Guide). Representative images
225 were produced by generating standard deviation pixel projections of Z-stacks in Fiji.

226 To visualise and analyse Lamin A at super-resolution level, Z-stack images (0.1 μm
227 increments) were acquired with a 100x oil objective (numerical aperture 1.5) and a Nikon
228 instant Structured Illumination Microscope (iSIM) system. At least six fibres were imaged per
229 individual, with each image including 1-7 myonuclei. To improve contrast and resolution (by
230 two-fold compared to confocal microscopy), iSIM images were deconvolved using inbuilt
231 algorithms in Nikon Elements software (3D Blind algorithm with 15 iterations and spherical
232 aberration correction) (York *et al.*, 2013; Curd *et al.*, 2015). The organisation of the nuclear
233 lamina was analysed using Fiji software. Line scan analysis of Lamin A staining was performed
234 by using the plot profile tool. Nuclear lamina deposition (arbitrary units) was quantified by using
235 a full width at half maximum macro to fit a Gaussian curve to pixel intensity profiles of Lamin
236 A stains. Measurements using the tool were taken in mid-focal planes, with an average taken

237 **Table 2. Antibodies and direct stains used in immunofluorescence experiments**

Antibody/ stain	Concentration	Company/Lab	Catalogue Number	Species
Lamin A	1:500	Sigma-Aldrich	L1293	Rabbit
Nesprin-1 (8C3)	1:400	Glen Morris lab	-	Rabbit
MYH7 (A4.951)	1:50	Santa Cruz Biotechnology	sc-53090	Mouse
α-Actinin (EA-53)	1:500	Sigma-Aldrich	A7811	Mouse
Alexa Fluor™ 594 Phalloidin	1:100	Invitrogen	A12381	-
Alexa Fluor™ 488 Goat anti-Rabbit IgG H+L	1:800	Invitrogen	A-11008	Goat
Alexa Fluor™ 555 Goat anti-Mouse IgG H+L Superclonal	1:800	Jackson Immunoresearch	715-165-150	Goat
Alexa Fluor™ 647 Goat anti-Mouse IgG H+L	1:800	Invitrogen	A-21235	Goat
Hoechst 33342	1:800	Invitrogen	H3570	-
DAPI	1:800	Molecular Probes	D3571	-

238

239 from a minimum of 6 measurements per nuclei. For nuclear invagination length analysis, a Fiji
240 plugin called Ridge Detection was used (Steger, 1998).

241 Assessment of myonuclear mechanics in single muscle fibres

242 To assess myonuclear mechanics in single muscle fibres, the extent of nuclear deformation
243 with increasing fibre tension was quantified (Shah & Lieber, 2003; Chapman *et al.*, 2014).
244 Muscle fibres from OT and OU were stretched to different tensions, fixed, and stained with
245 Hoechst and α-Actinin to visualise myonuclei and Z-discs of sarcomeres, respectively. Images
246 were acquired as before for 2D analysis, and sarcomere length was correlated with nuclear
247 aspect ratio, to assess myonuclear shape at various extents of muscle fibre stretch.

248 To determine stiffness, elastic, and viscosity properties of myonuclei, nanoindentation was
249 carried out on mounted single muscle fibres. Experiments were performed using an Optics11
250 Chiaro nanoindenter attached to a Leica DMI-8 inverted microscope. Mounted muscle fibres
251 were stained with Hoescht to locate myonuclei, and only nuclei at the nearest surface of the
252 muscle fibre to the indenter were analysed. Nanoindentation was performed with a 9 μm
253 diameter spherical probe (2.1 μm contact radius at 0.5 μm indentation depth, corresponding
254 to approximately half the nuclear radius, whereby an indentation at 0.5 μm depth measures
255 primarily the nuclear vs the cytoskeletal contribution to the stiffness (Guerrero *et al.*, 2019)).
256 Approach and retraction speeds were set to 500 nm/s. The Hertzian contact model was used
257 to fit the load-indentation data for calculation of Young's modulus.

258 Dynamic Mechanical Analysis (DMA), which uses a cyclic motion with frequency while
259 controlling displacement or load, was used to calculate the frequency-dependent storage
260 modulus (E'), loss modulus (E''), and the dissipation factor tan delta (E'/E'') of myonuclei,
261 corresponding to the elastic properties of nuclei. 1, 2, 4 and 10 Hz frequencies were used
262 (Table 3).

263 Mouse high intensity interval training programme

264 Animal handling

265 Twenty-four male ten-week-old C57BL/6 mice were maintained in groups of four in cages,
266 lined with wood shavings, cardboard rolls and cleaned weekly, in an automated room for
267 photoperiod control (light-dark cycle 12 h/ 12 h). Animals were provided with water and a
268 standard chow diet *ad libitum*. 12 mice were trained on treadmill over 8 weeks, with a
269 complementary sedentary group left in cages for an equivalent time-period. At the end of the
270 8 weeks, mice were sacrificed by cervical dislocation and *tibialis anterior* muscle was excised
271 from both legs of each mouse. Muscle from one leg was placed in skinning solution before

272 **Table 3. Dynamic mechanical analysis parameters for nanoindentation**

Frequency (Hz)	Indentation depth (nm)	Periods	Time (s)
1	500	5	2
2	500	5	2
4	500	20	2
10	500	20	2

273

274 cryopreservation and storage at -80 ℃ for later analysis through nanoindentation. Muscle from
275 the contralateral leg was snap frozen in liquid nitrogen for western blot analysis.

276 Treadmill familiarisation, determination of peak running velocity and training 277 programme

278 Mice were familiarised to the treadmill with five days of low intensity running (5 cm/s on the
279 first day, increasing the speed by 5 cm/s on the second, third, and fifth day, to end with a
280 speed of 20 cm/s). Treadmill incline was set at 0° on day one, 5° on days two and three, and
281 10° on day five. Peak running velocity (VPeak) was determined to estimate maximal aerobic
282 capacity and allow standardisation of the intensity of running during the training programme.
283 Exercise prescription based on VPeak and $\dot{V}O_2$max result in similar aerobic adaptations in
284 both humans and mice (Manoel *et al.*, 2017; Picoli *et al.*, 2018). VPeak was determined based
285 on the method outlined by Picoli et al. (Picoli *et al.*, 2018), adapted to incorporate a ramp,
286 rather than incremental, increase in running speed, as suggested by Ayachi et al. (Ayachi *et*
287 *al.*, 2016). Testing commenced with a warm-up for 4 min at 10 cm/s, before increasing the
288 speed gradually to 19 cm/s over the next minute (approximately 1 cm/s every 6.5 seconds).
289 Running speed was then increased by 1 cm/s every 20 seconds until exhaustion,
290 characterised by incapacity to keep running for more than 5 s (Mille-Hamard *et al.*, 2012).

291 Mice ran four times per week for eight weeks, based on a programme that showed ~50%
292 improvement in $\dot{V}O_2$max (Kemi *et al.*, 2002; Høydal *et al.*, 2007). After a warm-up at 10 cm/s
293 for 6 min, mice ran at approximately 80-90% Vpeak for three bouts of 8 min intermitted by 2
294 min active recovery at 50-60% Vpeak. Table 4 shows the speed and inclines of the training
295 programme. Muscle was excised from mice (sacrificed by cervical dislocation) 72 hours after
296 the final exercise session to exclude potential confounding effects observed acutely after
297 exercise (Carmichael *et al.*, 2005; Neubauer *et al.*, 2014).

298 Quantification of mouse skeletal muscle protein content by western 299 blotting

300 Tissue samples were lysed in 5M Urea, 2M Thiourea, 3% SDS, 75mM DTT, 0.03%
301 Bromophenol Blue, and 0.05M Tris HCl, and homogenised in a Precellys 24 tissue
302 homogeniser machine kept at 4°C. Samples were then sonicated for additional
303 homogenisation and shearing of DNA. For western blotting, frozen tissue lysates were thawed
304 and proteins linearised in a heating block at 95°C for 8 minutes, before loading on 4-12% Bis-
305 Tris gels. Proteins were transferred onto nitrocellulose membranes and blocked in 5% non-fat
306 milk powder in Tris Buffered Saline with 0.1% Tween20 (TBS-T) at 4°C for 1 hour. The
307 membranes were then incubated with primary antibodies overnight at 4°C, washed in TBS-T

308 **Table 4. Speed and incline of treadmill throughout mouse high intensity interval training**
309 **programme**

		Speed (cm/s)			Incline (°)
		Group 1	**Group 2**	**Group 3**	
Week 1	Exercise	32, 33	29, 30	28, 29	5
	Active recovery	19	18	17	
Week 2	Exercise	34, 35	31, 32	30, 31	
	Active recovery	19	18	17	
Week 3	Exercise	36, 37	33, 34	32, 33	
	Active recovery	20	19	18	
Week 4	Exercise	38, 39	35, 36	34, 35	
	Active recovery	20	19	18	
Week 5	Exercise	40, 41	37, 38	36, 37	
	Active recovery	21	20	19	
Week 6	Exercise	40, 41, 43	38, 39, 40, 40	37, 38	10
	Active recovery	21	20	19	
Week 7	Exercise	44, 45, 46, 47	41, 42, 43, 44	40, 41, 42, 43	
	Active recovery	22	21	20	
Week 8	Exercise	48	46	45	
	Active recovery	23	22	21	

310

311 4 times, and subsequently incubated with secondary antibodies for 1 hour. After 4 washes,
312 membranes imaged using a LI-COR Odyssey® CLx imaging system. Antibodies used for
313 western blotting are outlined in Table 5.

314 Statistics

315 Based on an expected mean difference of 15% between young and elderly individuals, an
316 effect size of 1.8, $\alpha = 0.05$ and power $(1-\beta) = 0.8$, the required sample size was determined
317 as six individuals per group. This studied was powered based on nuclear aspect ratio as the
318 primary end-point measurement. Because there were no studies on nuclear shape changes
319 in human muscle fibres, the study was powered based on data showing increased aspect ratio
320 of this magnitude in muscle fibres from mice expressing mutant lamins compared to control
321 mice (Earle et al., 2020). To analyse whether an overall significant difference was present
322 between muscle fibres from the different human groups, two-way analysis of variance
323 (ANOVA) tests were carried out, followed by post-hoc Tukey tests to specify between which
324 myonuclei or muscle fibres group differences existed. Mean values for each individual were
325 used for two-way ANOVA. For correlation analyses, a simple linear regression was performed
326 to test if slopes were significantly non-zero and nonlinear straight-line regression analyses
327 were performed to compare the slopes of different conditions. Two tailed t-tests were carried
328 out to analyse differences in protein concentrations, and Young's modulus between myonuclei
329 from exercise trained and untrained mice. Mean values for each mouse were used for t-tests.
330 With categorical data, individual measurements (myonuclei or muscle fibres) and mean values
331 calculated from these measurements were plotted in the same graph, using SuperPlots(Lord
332 *et al.*, 2020). Individual measurements were plotted as smaller grey points and overall means
333 of each individual or mouse are plotted as larger coloured points. For all statistical tests,
334 $p < 0.05$ indicated significance and $p < 0.07$ was taken to indicate a trend (* $P < 0.05$, ** $P <$
335 0.01, *** $P < 0.001$). Data are presented as mean ± SD except mean ± SEM in Figure 5. All
336 data were statistically analysed using Prism 9 (GraphPad).

337 Precision and reproducibility of methods

338 The same image processing and initial thresholding parameters were used for each image for
339 quantification of nuclear shape, nuclear organisation, lamina deposition, nuclear envelope
340 protein organisation. To quantify the precision and accuracy of the methods used, repeat
341 measurements were taken and the standard deviation and coefficient of variation were
342 calculated. Three repeat measurements of three nuclei were carried out for nuclear aspect
343 ratio and nuclear area. The mean of the standard deviation and coefficient of variation values
344 were then calculated to give a single standard deviation and coefficient of variation value for
345 nuclear aspect ratio and nuclear area. Five repeat measurements of sarcomere length were

346 **Table 5. Antibodies used for western blotting**

Antibody	Company/Lab	Catalogue Number	Species
Nesprin-1 (8C3)	Glen Morris Lab	-	Mouse
Nesprin-2	Didier Hodzic Lab	-	Rabbit
SUN1	Abcam	ab103021	Rabbit
SUN2	Didier Hodzic Lab	-	Rabbit
Lamin A/C	Larry Gerace Lab	-	Rabbit
Lamin B1	Larry Gerace Lab	-	Rabbit
Lamin B2	Abcam	ab151735	Rabbit
Emerin	Santa Cruz Biotechnologies	FL-254	Rabbit
Histone H3 (D1H2)	Cell Signaling Technology	4499T	Rabbit
IRDye® 680RD Donkey anti-Mouse IgG secondary antibody	LI-COR Biosciences	926-68072	Donkey
IRDye® 800CW Donkey anti-Rabbit IgG secondary antibody	LI-COR Biosciences	926-32213	Donkey

taken, and five repeat full width at half-maximum measurements of the nuclear lamina were carried out for assessment of the precision of lamina deposition. The standard deviation and coefficient of variation values were 0.02 and 0.67 for nuclear aspect ratio, 1.19 and 1.46 for nuclear area, 0.07 and 0.28 for sarcomere length, and 0.004 and 1.53 for lamina deposition, respectively.

Results

Myonuclei in both younger and older trained individuals are more spherical compared to untrained counterparts

Nuclei from laminopathy patients with premature ageing and muscle dysfunction are known to be ruffled and elongated (Goldman *et al.*, 2004; Park *et al.*, 2009; Tan *et al.*, 2015; Earle *et al.*, 2020). Here, we hypothesised that myonuclei would show similar abnormalities in physiological ageing. To investigate the effects of age and exercise training on myonuclear shape, muscle fibres were isolated from vastus lateralis biopsies taken from younger untrained (YU, 33 ± 9.5 years), younger trained (YT, 32 ± 5.4 years), older untrained (OU, 79 ± 11.3 years), and older trained (OT, 76 ± 3 years old) individuals.

In contrast to our hypothesis, myonuclei were strikingly rounder in shape in both younger and older trained individuals (Figure 1A), consistent with recent reports in rodents (Murach *et al.*, 2020; Rader & Baker, 2022). Indeed, the aspect ratio of myonuclei from trained individuals was ~27-29% lower than untrained counterparts, demonstrating significant differences in roundness (YU, 2.4 ± 0.3; OU, 2.3 ± 0.3; YT, 1.7 ± 0.1; OT, 1.6 ± 0.2; Figure 1B). To control for possible differences in fibre tension that may confound interpretation, we normalised myonuclear aspect ratio to sarcomere length and importantly found no differences associated with sarcomere length (Figure 1C). Sarcomere length was 2.0 ± 0.2 μm, 2.1 ± 0.2 μm, 2.0 ± 0.07 μm, and 2.2 ± 0.4 μm in YU, OU, YT, and OT, respectively. As further controls, exercise-dependent alterations to myonuclear shape remained apparent in slow muscle fibres expressing Myosin Heavy Chain 7, indicating that fibre-type differences between groups did not influence the effects observed (Figure 1D). In contrast to changes in nuclear aspect ratio, nuclear area was comparable in muscle fibres from trained and untrained individuals, highlighting that differences to myonuclear aspect ratio were driven by in myonuclear shape rather than size (Figure 1E).

Next, we performed 3D shape analysis of myonuclei by acquiring serial optical z-slices through whole muscle fibres (Figure 2A-B). In line with 2D shape changes observed, myonuclei from OT displayed a significant reduction in 3D aspect ratio compared to OU, with a trending reduction observed in YT compared to YU ($P < 0.07$) (Figure 2C). Furthermore, sphericity values were higher in trained individuals compared to age-matched untrained counterparts, indicating nuclei were more spherical in these groups (Figure 2D). Importantly, nuclear volumes were comparable across groups, consistent with our 2D analyses (Figure 2E).

Taken together, 2D and 3D analyses of myonuclear shape revealed striking morphological differences in younger and older trained individuals compared to untrained counterparts.

387 Nuclear lamina deposition is greater in skeletal muscle fibres from trained
388 individuals

389 Lamin A localisation and levels regulate nuclear stiffness and nuclear roundness (Lammerding
390 *et al.*, 2006; Swift *et al.*, 2013; Earle *et al.*, 2020; Srivastava *et al.*, 2021). Additionally, it has
391 recently been shown that a *Lmna* congenital muscular dystrophy alters mechanotransduction
392 in cultured myotubes and attenuates the hypertrophic response to functional overload in
393 mouse skeletal muscle *in vivo*, implicating a role of Lamin A/C in exercise adaptations (Owens
394 *et al.*, 2021). Thus, to investigate whether exercise affects the organisation of Lamin A in
395 skeletal muscle, muscle fibres from YU, YT, OU and OT individuals were stained with a Lamin
396 A-specific antibody (Figure 3). As expected, Lamin A localised to the periphery of myonuclei
397 (Figure 3A). Importantly, we observed a significant increase in nuclear lamina deposition in
398 myonuclei from OT compared to OU (Figure 4B-C). Next, we quantified nuclear invaginations,
399 which are tube-like infoldings of the nuclear envelope and are reported to play roles in
400 premature ageing syndromes (McClintock *et al.*, 2006; Frost, 2016; Schoen *et al.*, 2017).
401 However, our data showed there were no significant differences in total invagination length
402 (μm) between myonuclei from all groups (Figure 4D-E).

403 These data suggest that training is associated with increased nuclear lamina deposition in
404 primary human skeletal muscle.

405 Lamin A levels are increased in exercise-trained mice

406 Given the precious nature and paucity of human muscle biopsy samples for protein and
407 biophysical analysis, next we used a mouse model to investigate the effects of exercise on
408 myonuclear parameters further.

409 To determine whether exercise affected the protein levels of nuclear lamins and LINC complex
410 proteins, we performed western blotting on tibialis anterior muscle tissue from mice following
411 8 weeks of treadmill running. In line with increased Lamin A deposition in trained human
412 muscle fibres, Lamin A levels were significantly increased in trained mice compared to
413 untrained counterparts (442 ± 53 vs 384 ± 33, respectively, $P < 0.05$; Figure 4A). In contrast,
414 levels of Lamins C, B1, and Emerin were not significantly different (Figure 4A). LINC complex
415 proteins, which connect the cytoskeleton to the nucleus via the nuclear lamina, were then
416 analysed. Consistent with the increase in Lamin A, levels of SUN2, which is known to
417 preferentially bind Lamin A over Lamin C (Liang *et al.*, 2011), showed a 45% increase in
418 trained mice that was trending towards significance (1129 ± 498 vs 1639 ± 394, respectively,
419 $P = 0.055$). However, other LINC complex proteins SUN1, Nesprin-1α2 and Nesprin-2α1 were
420 not significantly different in trained compared to untrained mice (Figure 4B).

421 Exercise alters myonuclear deformability and stiffness

422 Changes in nuclear shape and Lamin A expression are associated with altered nuclear
423 mechanosensitivity, with Lamin A being a key regulator of the mechanical stiffness of nuclei
424 (Lammerding *et al.*, 2006). Thus, we next addressed whether structural alterations in
425 myonuclei from trained individuals translated to biophysical changes in nuclear mechanics.
426 Whilst it is accepted that adaptations to exercise are at least in part driven by
427 mechanotransduction (Hornberger & Esser, 2004; Kirby, 2019; Attwaters & Hughes, 2022),
428 the role of nuclear mechanics in this context has not previously been investigated.

429 To assess the effects of exercise on myonuclear function, myonuclear deformability was
430 compared in OU and OT human samples. Single muscle fibres were mounted and stretched
431 to different tensions, fixed, and stained to visualise myonuclei and Z-discs (Figure 5A)
432 (adapted from Chang et al., 2010; Chapman et al., 2014). We reasoned that if nuclear aspect
433 ratio increased proportionately with sarcomere length, nuclei were considered compliant with
434 fibre tension; conversely, if nuclear aspect ratio did not scale with sarcomere length, they were
435 considered stiffer. As expected, in both OT and OU fibres, there was a positive relationship
436 between sarcomere length and nuclear aspect ratio (R values were 0.36 and 0.45 for OT and
437 OU, respectively; 211 OT and 260 OU nuclei analysed, respectively; $P < 0.05$; Figure 5B).
438 However, this relationship was significantly steeper in fibres from OU compared to OT
439 (gradients were 0.79 and 0.29, respectively, $P < 0.05$; Figure 5B). Additionally, the variance
440 of myonuclear aspect ratio normalised to sarcomere length was significantly higher in OU
441 compared to OT fibres, showing less consistency in myonuclear shape changes with
442 stretching in OU fibres (Figure 5C, $P < 0.05$).

443 These data suggest that nuclei in trained individuals were less compliant with increasing fibre
444 tension compared to OU fibres (Figure 5B). In other words, nuclei in fibres from trained
445 individuals appeared stiffer than in untrained individuals. To confirm this, we used a
446 nanoindenter (which precisely measures mechanical properties of small samples and cells) to
447 physically probe nuclei and directly test the effects of exercise on myonuclear mechanics
448 (Figure 5D-E). Indeed, we observed an 87% increase in Young's modulus (kPa) (a measure
449 of stiffness) in myonuclei from trained mice compared to untrained mice (trained 1.7 ± 0.9 vs
450 untrained 3.2 ± 1.3, $P < 0.05$; Figure 5F). Additionally, there was a significant difference in the
451 viscoelasticity, whereby tan δ, the fraction of the loss modulus (the viscous component) over
452 the storage modulus (the elastic component), was on average ~20% lower in exercise trained
453 mice at 1, 2 and 4 Hz DMA ($P < 0.05$), and 14% lower at 10 Hz DMA (not significant) (Figure
454 5G-I), indicating more elastic nuclei in the trained mice.

455 Taken together, analysis of nuclear mechanics in human and mouse muscle fibres indicated
456 that training reduced myonuclear deformability, increased myonuclear stiffness and elasticity.

457 **Discussion**

458 Muscle pathologies and premature ageing syndromes caused by mutations in nuclear lamina
459 and envelope proteins have revealed a common phenotype: abnormal nuclear shape and
460 defective mechanotransduction. However, whether similar structural and functional defects
461 occur with physiological ageing with and without exercise in human skeletal muscle had not
462 previously been investigated.

463 Our main findings are that exercise, regardless of age, is associated with more spherical, less
464 deformable myonuclei, with increased Lamin A levels and deposition at the nuclear lamina.
465 This implies that myonuclear mechanotransduction may have a role in governing exercise
466 adaptations (Figure 6A). Maintaining myonuclear structure and function through regular
467 exercise may be an important factor in preserving muscle function throughout the lifespan
468 (Figure 6B). Conversely, myonuclear dysfunction in untrained muscle may contribute to age-
469 related decline in muscle mass and function (Figure 6B). Below, possible mechanisms and
470 consequences of exercise-related and inactivity-related alterations in myonuclear structure
471 and mechanics will be discussed.

472 Greater myonuclear sphericity and stiffness in trained muscle fibres may be a result of the
473 increased Lamin A expression. Lamin A regulates myonuclear shape and mechanics in
474 muscle cells, with loss or misexpression of Lamin A resulting in myonuclear elongation and
475 increased deformability (Roman *et al.*, 2017; Earle *et al.*, 2020). Forces can also induce
476 conformational changes to nuclear envelope and lamina proteins, modulating the mechanical
477 properties of nuclei (Swift *et al.*, 2013; Guilluy *et al.*, 2014; Buxboim *et al.*, 2014). Thus,
478 increased Lamin A expression may be an initial response to exercise training, which causes
479 increased myonuclear sphericity and stiffness, and reduces myonuclear deformability in
480 trained muscle fibres.

481 The structural and mechanical alterations to myonuclei in trained individuals may have several
482 consequences beneficial to muscle fibre function (Figure 6). These alterations may be
483 underpinned by altered chromatin organisation and expression of genes important for
484 oxidative capacity or repression of atrophy (Ho et al., 2013; Fischer et al., 2016). More
485 spherical, stiffer myonuclei with increased Lamin A expression may have enhanced
486 transduction of forces via the nuclear lamina, which tethers chromatin (Schreiner *et al.*, 2015).
487 This may directly regulate the expression of genes important for exercise adaptations, by
488 stretching or compacting chromatin to alter transcription factor accessibility (Tajik *et al.*, 2016).
489 Additionally, increased nuclear stiffness and altered lamina composition could increase the
490 association between the nuclear lamina and nuclear pore complexes, resulting in greater
491 expansion of nuclear complexes in response to contractile forces (Zimmerli *et al.*, 2021). This

492 may facilitate activity of transcriptional co-factors Yes-associated protein/Transcriptional
493 coactivator with PDZ-binding motif (Yap/Taz), which translocate to the nucleus upon activation
494 and co-activate TEAD transcription factors (Galli *et al.*, 2015; Gabriel *et al.*, 2016). Yap/Taz
495 activity has been associated with muscle growth, and signalling pathways involved in both
496 endurance and resistance exercise adaptations, such as AMPK and AKT1 (Gabriel *et al.*,
497 2016). Thus, altered lamina composition in endurance-trained individuals could increase
498 lamina-nuclear pore complex associations, making nuclear pore complexes more sensitive to
499 contractile forces and allowing transcriptional co-activators to enter nuclei to modulate
500 exercise adaptations.

501 In addition to facilitating exercise adaptations, myonuclear remodelling in trained individuals
502 may be mechanoprotective. Conversely, nuclear defects driven by inactivity may be
503 detrimental for cellular function and health (Kalukula *et al.*, 2022). Thus, increased Lamin A
504 expression and stiffness, and reduced deformability of myonuclei in trained muscle fibres may
505 improve resilience against contractile forces during future exercise bouts.

506 The elongated shape and greater deformability of myonuclei in untrained individuals were
507 reminiscent of those in muscle fibres from humans and mice with muscular dystrophies
508 characterised by muscle wasting and dysfunction (Tan *et al.*, 2015; Earle *et al.*, 2020). Thus,
509 defective myonuclear structure and function due to inactivity may contribute to age-related
510 muscle dysfunction. Specifically, chromatin stretching in more compliant myonuclei may result
511 in expression of genes that contribute to muscle atrophy, which are elevated after two weeks
512 of inactivity (Jones *et al.*, 2004). Additionally, altered chromatin organisation may repress
513 genes encoding contractile or mitochondrial proteins, decreasing force production and
514 endurance capacity (Figure 6B). Deformable myonuclei in untrained individuals may be more
515 susceptible to nuclear envelope rupture, impacting cell health (Earle *et al.*, 2020; Kalukula *et*
516 *al.*, 2022). These possible consequences of myonuclear dysfunction in old age may
517 collectively contribute to impairments in muscle mass, strength, and endurance with age, and
518 be alleviated by exercise-mediated myonuclear remodelling (Figure 6B).

519 A possible consequence of altered Lamin A expression in untrained individuals is reduced
520 nucleo-cytoskeletal shuttling of mechanosensitive transcription factor MRTF-A (Ho et al.,
521 2013). In *Lmna* mutant muscular dystrophy mouse embryonic fibroblasts, nuclear envelope
522 protein Emerin is mislocalised, resulting in modulated Actin dynamics and reduced nucleo-
523 cytoplasmic shuttling and activity of MRTF-A (Ho et al., 2013). In untrained skeletal muscle,
524 reduced Lamin A content could modulate Emerin localisation and Actin dynamics to facilitate
525 MRTF-A translocation to the nucleus through nuclear pore complexes. Because MRTF-A

activates muscle-specific genes, this could be detrimental for muscle health and function (Selvaraj & Prywes, 2003; Cenik *et al.*, 2016).

A limitation of our work was the limited availability of human muscle biopsies from the four groups, which could be complemented with future studies. In the present investigation, the older untrained group was composed of hip fracture patients with other underlying health conditions (see Table 1) which may have influenced the observed myonuclear aberrations. Participants were mixed sex, and drug administration and variations in habitual dietary intake were not stringently accounted for, possibly introducing variability in muscle fibre size and other variables. To this end, a study group composed of an older untrained group with clearer inclusion and exclusion criteria related to physical activity levels may provide a more accurate representation of the consequences of inactive ageing. Nevertheless, analysis of muscle fibres from this group has provided insight into myonuclear structure and function in elderly inactive individuals. Furthermore, these individuals displayed a strikingly similar nuclear shape phenotype to apparently healthy, younger untrained individuals.

The laborious and time-consuming nature of recruiting human participants and acquiring their samples for longitudinal studies makes cross-sectional analyses more feasible. To confirm our findings, a longitudinal study of myonuclear structure and function in samples serially acquired from active and inactive individuals throughout their lifespan would be required. This would provide a comprehensive account of the effects of active and inactive ageing on skeletal muscle myonuclei, and a causal relationship between changes in myonuclear parameters and muscle function.

In summary, our data suggest that exercise is associated with profound alterations in nuclear structure and mechanics in human primary muscle fibres regardless of age. In line with this, exercise resulted in increased Lamin A expression and myonuclear stiffness in mice. Future investigations into the potential role of myonuclear mechanotransduction in exercise and ageing would further our understanding of skeletal muscle physiology and offer new insights into improving human healthspan.

Additional information

Data availability statement

Individual datapoints ($n \leq 30$) are included in the figures. Data from the study will be made available upon reasonable request.

Competing interests

The authors have declared that no competing interests exist.

Author Contributions

MJS and JO contributed to the conception of the work. EB, JAR, MJS, and JO designed experiments. EB, JAR, AH, YH, and DGSW performed experiments. EB, AH, DGSW, and TI completed the formal analysis of the data. EB, JAR, AH, DGSW, TI, JO, and MJS interpreted the data. EB completed data visualisation. RDP, MK, JNP, GLC, NRL, SDRH and JO recruited human participants and collected human muscle biopsy samples. EB and MJS wrote the first draft of the manuscript. EB, JAR, AH, RDP, MK, GME, NRL, TI, SDRH, JO and MJS contributed to the manuscript and revised it critically. EB, JAR, AH, YH, DGSW, YL, RDP, MK, JNP, GLC, GME, NRL, TI, SDRH, JO and MJS approved the final version of the manuscript to be published. EB, JAR, AH, DGSW, YH, YL, RDP, MK, JNP, GLC, GME, NRL, TI, SDRH, JO and MJS agreed on all aspects of the work.

Funding

Julien Ochala and Edmund Battey are funded by the Medical Research Council of the UK (MR/S023593/1). Matthew J. Stroud is supported by British Heart Foundation Intermediate Fellowship: FS/17/57/32934 and King's BHF Centre for Excellence Award: RE/18/2/34213. Stephen D. R. Harridge, Norman R. Lazarus and Ross D. Pollock were funded by the Bupa Foundation. Michaeljohn Kalakoutis was funded by a King’s College London PhD studentship.

583 **References**

584 Attwaters M & Hughes SM (2022). Cellular and molecular pathways controlling muscle size in
585 response to exercise. *FEBS Journal* **289,** 1428–1456.

586 Ayachi M, Niel R, Momken I, Billat VL & Mille-Hamard L (2016). Validation of a ramp running
587 protocol for determination of the true VO2max in mice. *Front Physiol*; DOI:
588 10.3389/FPHYS.2016.00372/FULL.

589 Banerjee I, Zhang J, Moore-Morris T, Pfeiffer E, Buchholz KS, Liu A, Ouyang K, Stroud MJ,
590 Gerace L, Evans SM, McCulloch A & Chen J (2014). Targeted Ablation of Nesprin 1 and
591 Nesprin 2 from Murine Myocardium Results in Cardiomyopathy, Altered Nuclear
592 Morphology and Inhibition of the Biomechanical Gene Response. *PLoS Genet* **10,**
593 e1004114.

594 Battey E, Furrer R, Ross J, Handschin C, Ochala J & Stroud MJ (2022). PGC-1α regulates
595 myonuclear accretion after moderate endurance training. *J Cell Physiol* **237,** 696–705.

596 Battey E, Stroud MJ & Ochala J (2020). Using nuclear envelope mutations to explore age-
597 related skeletal muscle weakness. *Clin Sci* **134,** 2177–2187. Available at:
598 https://portlandpress.com/clinsci/article-abstract/134/16/2177/226196 [Accessed
599 February 16, 2021].

600 Bonne G, Schwartz K, Barletta MR di, Varnous S, Bécane H-M, Hammouda E-H, Merlini L,
601 Muntoni F, Greenberg CR, Gary F, Urtizberea J-A, Duboc D, Fardeau M & Toniolo D
602 (1999). Mutations in the gene encoding lamin A/C cause autosomal dominant Emery-
603 Dreifuss muscular dystrophy. *Nat Genet* **21,** 285–288.

604 Brown GC (2015). Living too long. *EMBO Rep* **16,** 137–141.

605 Buxboim A, Swift J, Irianto J, Spinler KR, Dingal PCDP, Athirasala A, Kao YRC, Cho S, Harada
606 T, Shin JW & Discher DE (2014). Matrix elasticity regulates lamin-A,C phosphorylation
607 and turnover with feedback to actomyosin. *Curr Biol* **24,** 1909–1917.

608 Carmichael MD, Davis JM, Murphy EA, Brown AS, Carson JA, Mayer E & Ghaffar A (2005).
609 Recovery of running performance following muscle-damaging exercise: Relationship to
610 brain IL-1β. *Brain Behav Immun* **19,** 445–452.

611 Cenik BK, Liu N, Chen B, Bezprozvannaya S, Olson EN & Bassel-Duby R (2016). Myocardin-
612 related transcription factors are required for skeletal muscle development. *Development*
613 *(Cambridge)* **143,** 2853–2861.

614 Chapman MA, Zhang J, Banerjee I, Guo LT, Zhang Z, Shelton GD, Ouyang K, Lieber RL &
615 Chen J (2014). Disruption of both nesprin 1 and desmin results in nuclear anchorage
616 defects and fibrosis in skeletal muscle. *Hum Mol Genet* **23,** 5879–5892.

617 Cho S, Irianto J & Discher DE (2017). Mechanosensing by the nucleus: From pathways to
618 scaling relationships. *Journal of Cell Biology* **216,** 305–315.

619 Crisp M, Liu Q, Roux K, Rattner JB, Shanahan C, Burke B, Stahl PD & Hodzic D (2006).
620 Coupling of the nucleus and cytoplasm: Role of the LINC complex. *Journal of Cell Biology*
621 **172,** 41–53.

622 Cupesi M, Yoshioka J, Gannon J, Kudinova A, Stewart CL & Lammerding J (2010). Attenuated
623 hypertrophic response to pressure overload in a lamin A/C haploinsufficiency mouse. *J*
624 *Mol Cell Cardiol* **48,** 1290–1297.

625 Curd A, Cleasby A, Makowska K, York A, Shroff H & Peckham M (2015). Construction of an
626 instant structured illumination microscope. *Methods* **88,** 37–47.

627 Earle AJ, Kirby TJ, Fedorchak GR, Isermann P, Patel J, Iruvanti S, Moore SA, Bonne G,
628 Wallrath LL & Lammerding J (2020). Mutant lamins cause nuclear envelope rupture and
629 DNA damage in skeletal muscle cells. *Nat Mater* **19,** 464–473.

630 Fischer M, Rikeit P, Knaus P & Coirault C (2016). YAP-mediated mechanotransduction in
631 skeletal muscle. *Front Physiol* **7,** 41.

632 Frontera WR & Larsson L (1997). Contractile studies of single human skeletal muscle fibers:
633 A comparison of different muscles, permeabilization procedures, and storage techniques.
634 *Muscle Nerve* **20,** 948–952.

635 Frost B (2016). Alzheimer's disease: An acquired neurodegenerative laminopathy. *Nucleus* **7,**
636 275–283.

637 Gabriel BM, Lee Hamilton D, Tremblay AM & Wackerhage H (2016). The Hippo signal
638 transduction network for exercise physiologists. *J Appl Physiol* **120,** 1105–1117.

639 Galli GG, Carrara M, Yuan WC, Valdes-Quezada C, Gurung B, Pepe-Mooney B, Zhang T,
640 Geeven G, Gray NS, de Laat W, Calogero RA & Camargo FD (2015). YAP Drives Growth
641 by Controlling Transcriptional Pause Release from Dynamic Enhancers. *Mol Cell* **60,**
642 328–337.

643 Gerhart-Hines Z, Rodgers JT, Bare O, Lerin C, Kim SH, Mostoslavsky R, Alt FW, Wu Z &
644 Puigserver P (2007). Metabolic control of muscle mitochondrial function and fatty acid
645 oxidation through SIRT1/PGC-1α. *EMBO J* **26,** 1913–1923.

646 Goldman RD, Shumaker DK, Erdos MR, Eriksson M, Goldman AE, Gordon LB, Gruenbaum
647 Y, Khuon S, Mendez M, Varga R & Collins FS (2004). Accumulation of mutant lamin A
648 causes progressive changes in nuclear architecture in Hutchinson–Gilford progeria
649 syndrome. *Proceedings of the National Academy of Sciences* **101,** 8963–8968.

650 Greig CA, Young A, Skelton DA, Pippet E, Butler FMM & Mahmud SM (1994). Exercise studies
651 with elderly volunteers. *Age Ageing* **23,** 185–189.

652 Guerrero CR, Garcia PD & Garcia R (2019). Subsurface Imaging of Cell Organelles by Force
653 Microscopy. *ACS Nano* **13,** 9629–9637.

654 Guilluy C, Osborne LD, van Landeghem L, Sharek L, Superfine R, Garcia-Mata R & Burridge
655 K (2014). Isolated nuclei adapt to force and reveal a mechanotransduction pathway in
656 the nucleus. *Nat Cell Biol* **16,** 376–381.

657 Gurd BJ (2011). Deacetylation of PGC-1a by SIRT1: Importance for skeletal muscle function
658 and exercise-induced mitochondrial biogenesis. *Applied Physiology, Nutrition and*
659 *Metabolism* **36,** 589–597. Available at: www.nrcresearchpress.com [Accessed April 17,
660 2022].

661 Guthold R, Stevens GA, Riley LM & Bull FC (2018). Worldwide trends in insufficient physical
662 activity from 2001 to 2016: a pooled analysis of 358 population-based surveys with 1·9
663 million participants. *Lancet Glob Health* **6,** e1077–e1086.

664 Ho CY, Jaalouk DE, Vartiainen MK & Lammerding J (2013*a*). Lamin A/C and emerin regulate
665 MKL1-SRF activity by modulating actin dynamics. *Nature* **497,** 507–511.

666 Ho CY, Jaalouk DE, Vartiainen MK & Lammerding J (2013*b*). Lamin A/C and emerin regulate
667 MKL1-SRF activity by modulating actin dynamics. *Nature* **497,** 507–513.

668 Hornberger TA & Esser KA (2004). Mechanotransduction and the regulation of protein
669 synthesis in skeletal muscle. *Proceedings of the Nutrition Society* **63,** 331–335.

670 Høydal MA, Wisløff U, Kemi OJ & Ellingsen Ø (2007). Running speed and maximal oxygen
671 uptake in rats and mice: practical implications for exercise training. *European journal of*
672 *cardiovascular prevention and rehabilitation* **14,** 753–760.

673 Janin A, Bauer D, Ratti F, Millat G & Méjat A (2017). Nuclear envelopathies: A complex LINC
674 between nuclear envelope and pathology. *Orphanet J Rare Dis* **12,** 1–16. Available at:
675 https://ojrd.biomedcentral.com/articles/10.1186/s13023-017-0698-x [Accessed April 18,
676 2022].

677 Jones SW, Hill RJ, Krasney PA, O'Conner B, Peirce N & Greenhaff PL (2004). Disuse atrophy
678 and exercise rehabilitation in humans profoundly affects the expression of genes
679 associated with the regulation of skeletal muscle mass. *The FASEB Journal* **18,** 1025–
680 1027.

681 Kalukula Y, Stephens AD, Lammerding J & Gabriele S (2022). Mechanics and functional
682 consequences of nuclear deformations. *Nature Reviews Molecular Cell Biology 2022*1–
683 20.

684 Kemi OJ, Loennechen JP, Wisløff U & Ellingsen Y (2002). Intensity-controlled treadmill
685 running in mice: Cardiac and skeletal muscle hypertrophy. *J Appl Physiol* **93,** 1301–1309.

686 Kirby TJ (2019). Mechanosensitive pathways controlling translation regulatory processes in
687 skeletal muscle and implications for adaptation. *J Appl Physiol* **127,** 608–618.

688 Kirby TJ & Lammerding J (2018). Emerging views of the nucleus as a cellular mechanosensor.
689 *Nat Cell Biol* **20,** 373–381.

690 Konigsberg UR, Lipton BH & Konigsberg IR (1975). The regenerative response of single
691 mature muscle fibers isolated in vitro. *Dev Biol* **45,** 260–275.

692 Lammerding J, Fong LG, Ji JY, Reue K, Stewart CL, Young SG & Lee RT (2006). Lamins a
693 and C but not lamin B1 regulate nuclear mechanics. *Journal of Biological Chemistry* **281,**
694 25768–25780.

695 Lazarus NR & Harridge SDR (2017). Declining performance of master athletes: silhouettes of
696 the trajectory of healthy human ageing? *Journal of Physiology* **595,** 2941–2948.

697 Lazarus NR, Lord JM & Harridge SDR (2019). The relationships and interactions between
698 age, exercise and physiological function. *Journal of Physiology* **597,** 1299–1309.

699 Levy Y, Ross JA, Niglas M, Snetkov VA, Lynham S, Liao C-Y, Puckelwartz MJ, Hsu Y-M,
700 McNally EM, Alsheimer M, Harridge SDR, Young SG, Fong LG, Español Y, Lopez-Otin
701 C, Kennedy BK, Lowe DA & Ochala J (2018). Prelamin A causes aberrant myonuclear
702 arrangement and results in muscle fiber weakness. *JCI Insight* **3,** 1–18.

703 Liang Y, Chiu PH, Yip KY & Chan SY (2011). Subcellular localization of SUN2 is regulated by
704 lamin a and Rab5. *PLoS One*; DOI: 10.1371/journal.pone.0020507.

705 Little JP, Safdar A, Wilkin GP, Tarnopolsky MA & Gibala MJ (2010). A practical model of low-
706 volume high-intensity interval training induces mitochondrial biogenesis in human
707 skeletal muscle: potential mechanisms. *J Physiol* **588,** 1011–1022.

708 Lord SJ, Velle KB, Dyche Mullins R & Fritz-Laylin LK (2020). SuperPlots: Communicating
709 reproducibility and variability in cell biology. *Journal of Cell Biology*; DOI:
710 10.1083/JCB.202001064.

711 Maggi L, Carboni N & Bernasconi P (2016). Skeletal Muscle Laminopathies: A Review of
712 Clinical and Molecular Features. *Cells* **5,** 33.

713 Manoel F, da Silva D, Lima J & Machado F (2017). Peak velocity and its time limit are as good
714 as the velocity associated with VO2max for training prescription in runners. *Sports Med*
715 *Int Open* **01,** E8–E15.

716 Maurer M & Lammerding J (2019). The Driving Force: Nuclear Mechanotransduction in
717 Cellular Function, Fate, and Disease. *Annu Rev Biomed Eng* **21,** annurev-bioeng-
718 060418-052139.

719 McClintock D, Gordon LB & Djabali K (2006). Hutchinson-Gilford progeria mutant lamin A
720 primarily targets human vascular cells as detected by an anti-Lamin A G608G antibody.
721 *Proc Natl Acad Sci U S A* **103,** 2154–2159.

722 Merideth MA et al. (2008). Phenotype and course of Hutchinson-Gilford progeria syndrome.
723 *New England Journal of Medicine* **358,** 592–604.

724 Mille-Hamard L, Billat VL, Henry E, Bonnamy B, Joly F, Benech P & Barrey E (2012). Skeletal
725 muscle alterations and exercise performance decrease in erythropoietin-deficient mice:
726 A comparative study. *BMC Med Genomics*; DOI: 10.1186/1755-8794-5-29.

727 Murach KA, Mobley CB, Zdunek CJ, Frick KK, Jones SR, McCarthy JJ, Peterson CA &
728 Dungan CM (2020). Muscle memory: myonuclear accretion, maintenance, morphology,
729 and miRNA levels with training and detraining in adult mice. *J Cachexia Sarcopenia*
730 *Muscle* **11,** 1705–1722.

731 Neubauer O, Sabapathy S, Ashton KJ, Desbrow B, Peake JM, Lazarus R, Wessner B,
732 Cameron-Smith D, Wagner KH, Haseler LJ & Bulmer AC (2014). Time course-dependent
733 changes in the transcriptome of human skeletal muscle during recovery from endurance
734 exercise: From inflammation to adaptive remodeling. *J Appl Physiol* **116,** 274–287.

735 Nikitara K, Odani S, Demenagas N, Rachiotis G, Symvoulakis E & Vardavas C (2021).
736 Prevalence and correlates of physical inactivity in adults across 28 European countries.
737 *Eur J Public Health* **31,** 840–845.

738 Osmanagic-Myers S, Dechat T & Foisner R (2015). Lamins at the crossroads of
739 mechanosignaling. *Genes Dev* **29,** 225–237.

740 Owens DJ, Messéant J, Moog S, Viggars M, Ferry A, Mamchaoui K, Lacène E, Roméro N,
741 Brull A, Bonne G, Butler-Browne G & Coirault C (2021). Lamin-related congenital
742 muscular dystrophy alters mechanical signaling and skeletal muscle growth. *Int J Mol Sci*
743 **22,** 1–22.

744 Park YE, Hayashi YK, Goto K, Komaki H, Hayashi Y, Inuzuka T, Noguchi S, Nonaka I &
745 Nishino I (2009). Nuclear changes in skeletal muscle extend to satellite cells in autosomal
746 dominant Emery-Dreifuss muscular dystrophy/limb-girdle muscular dystrophy 1B.
747 *Neuromuscular Disorders* **19,** 29–36.

748 Piccus R & Brayson D (2020). The nuclear envelope: LINCing tissue mechanics to genome
749 regulation in cardiac and skeletal muscle. *Biol Lett*; DOI: 10.1098/rsbl.2020.0302.
750 Available at: https://royalsocietypublishing.org/doi/10.1098/rsbl.2020.0302 [Accessed
751 September 20, 2022].

752 Picoli C de C, Romero PV da S, Gilio GR, Guariglia DA, Tófolo LP, de Moraes SMF, Machado
753 FA & Peres SB (2018). Peak velocity as an alternative method for training prescription in
754 mice. *Front Physiol*; DOI: 10.3389/fphys.2018.00042.

755 Pollock RD, Carter S, Velloso CP, Duggal NA, Lord JM, Lazarus NR & Harridge SDR (2015).
756 An investigation into the relationship between age and physiological function in highly
757 active older adults. *Journal of Physiology* **593,** 657–680.

758 Pollock RD, O'Brien KA, Daniels LJ, Nielsen KB, Rowlerson A, Duggal NA, Lazarus NR, Lord
759 JM, Philp A & Harridge SDR (2018). Properties of the vastus lateralis muscle in relation
760 to age and physiological function in master cyclists aged 55–79 years. *Aging Cell*; DOI:
761 10.1111/acel.12735.

762 Rader EP & Baker BA (2022). Elevated muscle mass accompanied by transcriptional and
763 nuclear alterations several months following cessation of resistance-type training in rats.
764 *Physiol Rep* **10,** e15476.

765 Roman W, Martins JP, Carvalho FA, Voituriez R, Abella JVG, Santos NC, Cadot B, Way M &
766 Gomes ER (2017). Myofibril contraction and crosslinking drive nuclear movement to the
767 periphery of skeletal muscle. *Nat Cell Biol* **19,** 1189–1201.

768 Ross JA et al. (2019). Impairments in contractility and cytoskeletal organisation cause nuclear
769 defects in nemaline myopathy. *Acta Neuropathol* **138,** 477–495.

770 Ross JA, Pearson A, Levy Y, Cardel B, Handschin C & Ochala J (2017). Exploring the Role
771 of PGC-1α in Defining Nuclear Organisation in Skeletal Muscle Fibres. *J Cell Physiol* **232,**
772 1270–1274.

773 Ross JA & Stroud MJ (2021). THE NUCLEUS: Mechanosensing in cardiac disease.
774 *International Journal of Biochemistry and Cell Biology* **137,** 106035.

775 Schindelin J, Arganda-Carreras I, Frise E, Kaynig V, Longair M, Pietzsch T, Preibisch S,
776 Rueden C, Saalfeld S, Schmid B, Tinevez JY, White DJ, Hartenstein V, Eliceiri K,
777 Tomancak P & Cardona A (2012). Fiji: An open-source platform for biological-image
778 analysis. *Nat Methods* **9,** 676–682.

779 Schoen I, Aires L, Ries J & Vogel V (2017). Nanoscale invaginations of the nuclear envelope:
780 Shedding new light on wormholes with elusive function. *Nucleus* **8,** 506–514.

781 Schreiner SM, Koo PK, Zhao Y, Mochrie SGJ & King MC (2015). The tethering of chromatin
782 to the nuclear envelope supports nuclear mechanics. *Nat Commun*; DOI:
783 10.1038/ncomms8159.

784 Selvaraj A & Prywes R (2003). Megakaryoblastic Leukemia-1/2, a Transcriptional Co-activator
785 of Serum Response Factor, is required for Skeletal Myogenic Differentiation. *Journal of*
786 *Biological Chemistry* **278,** 41977–41987.

787 Shah SB & Lieber RL (2003). Simultaneous Imaging and Functional Assessment of
788 Cytoskeletal Protein Connections in Passively Loaded Single Muscle Cells. *The Journal*
789 *of Histochemistry & Cytochemistry* **51,** 19–29.

790 Shen Z, Lengyel M, Niethammer P & Os Lengyel M (2022). The yellow brick road to nuclear
791 membrane mechanotransduction. *APL Bioeng* **6,** 021501.

792 Shin JY & Worman HJ (2021). Molecular Pathology of Laminopathies. *Annual Review of*
793 *Pathology: Mechanisms of Disease* **17,** 159–180.

794 Shur NF, Creedon L, Skirrow S, Atherton PJ, MacDonald IA, Lund J & Greenhaff PL (2021).
795 Age-related changes in muscle architecture and metabolism in humans: The likely
796 contribution of physical inactivity to age-related functional decline. *Ageing Res Rev* **68,**
797 101344.

798 Srivastava LK, Ju Z, Ghagre A & Ehrlicher AJ (2021). Spatial distribution of lamin A/C
799 determines nuclear stiffness and stress-mediated deformation. *J Cell Sci*; DOI:
800 10.1242/jcs.248559.

801 Steger G (1998). An unbiased detector of curvilinear structures. *IEEE Trans Pattern Anal*
802 *Mach Intell* **20,** 113–125.

803 Stienen GJM (2000). Chronicle of skinned muscle fibres. *Journal of Physiology* **527,** 1.

804 Stroud MJ (2018). Linker of nucleoskeleton and cytoskeleton complex proteins in
805 cardiomyopathy. *Biophys Rev* **10,** 1033–1051.

806 Stroud MJ, Feng W, Zhang J, Veevers J, Fang X, Gerace L & Chen J (2017). Nesprin 1α2 is
807 essential for mouse postnatal viability and nuclear positioning in skeletal muscle. *Journal*
808 *of Cell Biology* **216,** 1915–1924.

809 Swift J, Ivanovska IL, Buxboim A, Harada T, Dingal PCDP, Pinter J, Pajerowski JD, Spinler
810 KR, Shin JW, Tewari M, Rehfeldt F, Speicher DW & Discher DE (2013). Nuclear lamin-A
811 scales with tissue stiffness and enhances matrix-directed differentiation. *Science*; DOI:
812 10.1126/SCIENCE.1240104.

813 Tajik A, Zhang Y, Wei F, Sun J, Jia Q, Zhou W, Singh R, Khanna N, Belmont AS & Wang N
814 (2016). Transcription upregulation via force-induced direct stretching of chromatin. *Nat*
815 *Mater* **15,** 1287–1296.

816 Tan D, Yang H, Yuan Y, Bonnemann C, Chang X, Wang S, Wu Y, Wu X & Xiong H (2015).
817 Phenotype-genotype analysis of Chinese patients with early-onset LMNA-related
818 muscular dystrophy. *PLoS One*; DOI: 10.1371/journal.pone.0129699.

819 United. ND of E and SA (n.d.). World Population Prospects 2022 Summary of Results.

820 Wood DS, Zollman J, Reuben JP & Brandt PW (1975). Human skeletal muscle: Properties of
821 the “chemically skinned” fiber. *Science (1979)* **187,** 1075–1076.

822 Wroblewski AP, Amati F, Smiley MA, Goodpaster B & Wright V (2011). Chronic exercise
823 preserves lean muscle mass in masters athletes. *Physician and Sportsmedicine* **39,** 62.

824 York AG, Chandris P, Nogare DD, Head J, Wawrzusin P, Fischer RS, Chitnis A & Shroff H
825 (2013). Instant super-resolution imaging in live cells and embryos via analog image
826 processing. *Nat Methods* **10,** 1122–1130.

827 Zhang J, Felder A, Liu Y, Guo LT, Lange S, Dalton ND, Gu Y, Peterson KL, Mizisin AP, Shelton
828 GD, Lieber RL & Chen J (2010). Nesprin 1 is critical for nuclear positioning and
829 anchorage. *Hum Mol Genet* **19,** 329–341.

830 Zimmerli CE, Allegretti M, Rantos V, Goetz SK, Obarska-Kosinska A, Zagoriy I, Halavatyi A,
831 Hummer G, Mahamid J, Kosinski J & Beck M (2021). Nuclear pores dilate and constrict
832 in cellulo. *Science (1979)*; DOI: 10.1126/science.abd9776.

833

834

835 **Figure legends**

836 **Abstract figure: Structural and mechanical properties of myonuclei in trained young**
837 **and aged individuals.** In skeletal muscle fibres from trained individuals, myonuclei are more
838 spherical, have greater Lamin A and are stiffer compared to untrained counterparts. This may
839 protect nuclei from damage when subjected to contractile forces during exercise, and permit
840 effective transduction of these forces to regulate gene expression and signalling pathways
841 (mechanotransduction). In skeletal muscle from untrained older individuals, myonuclei are
842 more elongated, nuclear lamina levels are lower, and myonuclei are more deformable. This
843 may increase susceptibility to myonuclear damage and defective mechanotransduction,
844 contributing to declines in muscle mass and function.

845 **Figure 1: Altered 2D myonuclear shape in trained younger and older individuals** (A)
846 Representative images of vastus lateralis muscle fibres isolated from younger untrained (YU),
847 older untrained (OU), younger trained (YT) and older trained (OT) individuals, stained with
848 DAPI (cyan) and Myosin Heavy Chain 7 (magenta) to visualise myonuclei and slow myosin,
849 respectively. Scale bars 30 µm and 10 µm main images and zoomed insets of myonuclei,
850 respectively. (B-E) Calculation of aspect ratio (length/width of nucleus) and nuclear area (μm^2)
851 shown above graphs. (B) Comparisons of myonuclear aspect ratio in YU, OU, YT, and OT
852 individuals; 2053 total nuclei analysed (C) Comparisons of myonuclear aspect ratio between
853 groups after normalisation to sarcomere length (D) Myonuclear aspect ratio in MYH7+ fibres
854 (1385 total nuclei analysed) (E) Comparisons of nuclear area (μm^2) between groups (1453
855 total nuclei analysed). (B-E) Coloured symbols represent individual means, unfilled grey
856 symbols represent myonuclei; mean values for individuals were used for two-way ANOVA
857 tests (n = 6, ** $P < 0.01$ *** $P < 0.001$); error bars represent mean ± SD.

858 **Figure 2: Lower 3D aspect ratio and greater sphericity in myonuclei from trained**
859 **younger and older individuals** (A) Representative three-dimensional rendering of z-stack
860 images of a single human vastus lateralis muscle fibre acquired with a spinning disk confocal
861 microscope equipped with a 63x oil objective lens. Muscle fibre stained to visualise Lamin A
862 (cyan), DNA (magenta), Actin (green), Myosin Heavy Chain 7 (MYH7, red). (B) Representative
863 zoomed images of 3D-rendered nucleus. (C-E) Comparisons of nuclear skeletal length/
864 diameter (µm), sphericity, and volume in younger untrained (YU), older untrained (OU),
865 younger trained (YT) and older trained (OT) individuals. Coloured symbols represent individual
866 means, unfilled grey symbols represent myonuclei; mean values for individuals were used for
867 two-way ANOVA tests (n = 4-6, ** $P < 0.01$ *** $P < 0.001$ **** $P < 0.0001$); error bars represent
868 mean ± SD.

869 **Figure 3: Organisation of Lamin A in trained individuals and untrained counterparts** (A)
870 Representative images, acquired through confocal microscopy using a 63x oil objective, of
871 muscle fibres isolated from younger untrained (YU), older untrained (OU) patients, younger
872 trained (YT) and older untrained (OT). Fibres were stained with DAPI to visualise DNA (blue),
873 Actin (red), Lamin A (green, gray) and Myosin Heavy Chain 7 (MYH7, magenta). Scale bar 25
874 µm in main images, 10 µm in zoomed images. (B) Representative images of myonuclei from
875 OU and OT muscle fibres acquired through super resolution iSIM microscopy. Scale bars 5
876 µm. (C) Quantification of Lamin A deposition (µm) in muscle fibres from OT and OU. N = 3-5
877 per group, unpaired t-test revealed significant difference between groups ($P < 0.05$). (D)
878 Standard deviation projections of Lamin A-stained myonuclei and pixel intensity line scans
879 (yellow line) from YU, OU, YT, and OT. (E) Lamin A total invagination length (µm) in muscle
880 fibres from YU, OU, YT, OT, n = 6. Two-way ANOVA revealed no significant differences
881 between groups. Coloured symbols represent individual means, grey symbols represent
882 myonuclei; mean values for individuals were used for two-way ANOVA tests and t-test. Error
883 bars represent mean ± SD.

884 **Figure 4: Lamin A levels are increased in trained mouse tibialis anterior muscle** (A)
885 Protein levels of Lamin A, Lamin C, Lamin B1 and Emerin normalised to Histone H3 in tibialis
886 anterior muscle from untrained and high intensity endurance trained mice (B) Protein levels of
887 Linker of Nucleoskeleton and Cytoskeleton (LINC) complex proteins SUN1, SUN2, Nesprin-
888 1-α2, and Nesprin-2-α1 normalised to Histone H3 in tibialis anterior muscle from untrained
889 and trained mice (C-D) Images of western blots from which data in A-B were obtained. Note
890 that Lamin A levels were significantly increased and SUN2 levels trending to increase. Arrows
891 indicate predicted molecular weights (kD). Data points represent individual mice, n = 7 per
892 group, * indicates $P < 0.05$ (t-test). Error bars represent mean ± SD.

893 **Figure 5: Exercise training results in stiffer myonuclei** (A) Schematic of fibre mounting
894 and stretching. (B) Relationship between sarcomere length and nuclear aspect ratio in muscle
895 fibres from older trained (OT) and untrained (OU) patients. (C) Variance of aspect ratio/
896 sarcomere length in OT and OU fibres. Note that sarcomere length positively correlates with
897 extent of muscle fibre stretch and that myonuclei in OT fibres were significantly stiffer than
898 myonuclei from OU fibres. * denotes statistically significant difference between gradients of
899 slopes (linear regression analysis, F-test to compare variances). (D) Typical setup of individual
900 muscle fibres after isolation and mounting in parallel on an electron microscopy (EM) grid split
901 in half for imaging and nanoindentation. (E) Nanoindentation of single muscle fibres
902 (brightfield) with myonuclei labelled (green) being probed by nanoindenter (brightfield, left of
903 image). Scale bar, 50 µm. (F) Comparison of Young's modulus (kPa) in nuclei from untrained

904 (red) and trained mice (blue) (G-I) comparisons of E', E'' and Tan Delta (E"/E') at different
905 Dynamic Mechanical Analysis (DMA) frequencies (Hz) in nuclei from untrained and exercise
906 trained mice. Note that myonuclei were significantly more stiff and more elastic in fibres from
907 trained vs. untrained mice. Each coloured data point represents the average for each mouse,
908 n = 3 per group. Error bars represent mean ± SEM. * denotes statistically significant difference
909 between groups (t-test and mixed effects analysis).

910 **Figure 6: Summary and proposed effects of myonuclear remodelling with training, and**
911 **inactivity related defects in nuclear mechanotransduction with age** (A) In skeletal muscle
912 fibres from trained individuals, nuclear envelope proteins including the nuclear lamina
913 effectively transduce cytoskeletal forces to the nucleus to regulate signalling pathways. (B) In
914 skeletal muscle from trained older individuals, myonuclear shape and mechanotransduction
915 are preserved (C) In skeletal muscle from untrained older individuals, myonuclei are more
916 elongated, nuclear lamina levels are reduced, and myonuclei more deformable. This may lead
917 to increased susceptibility to myonuclear damage and defective mechanotransduction that
918 results in decline in muscle mass and function.

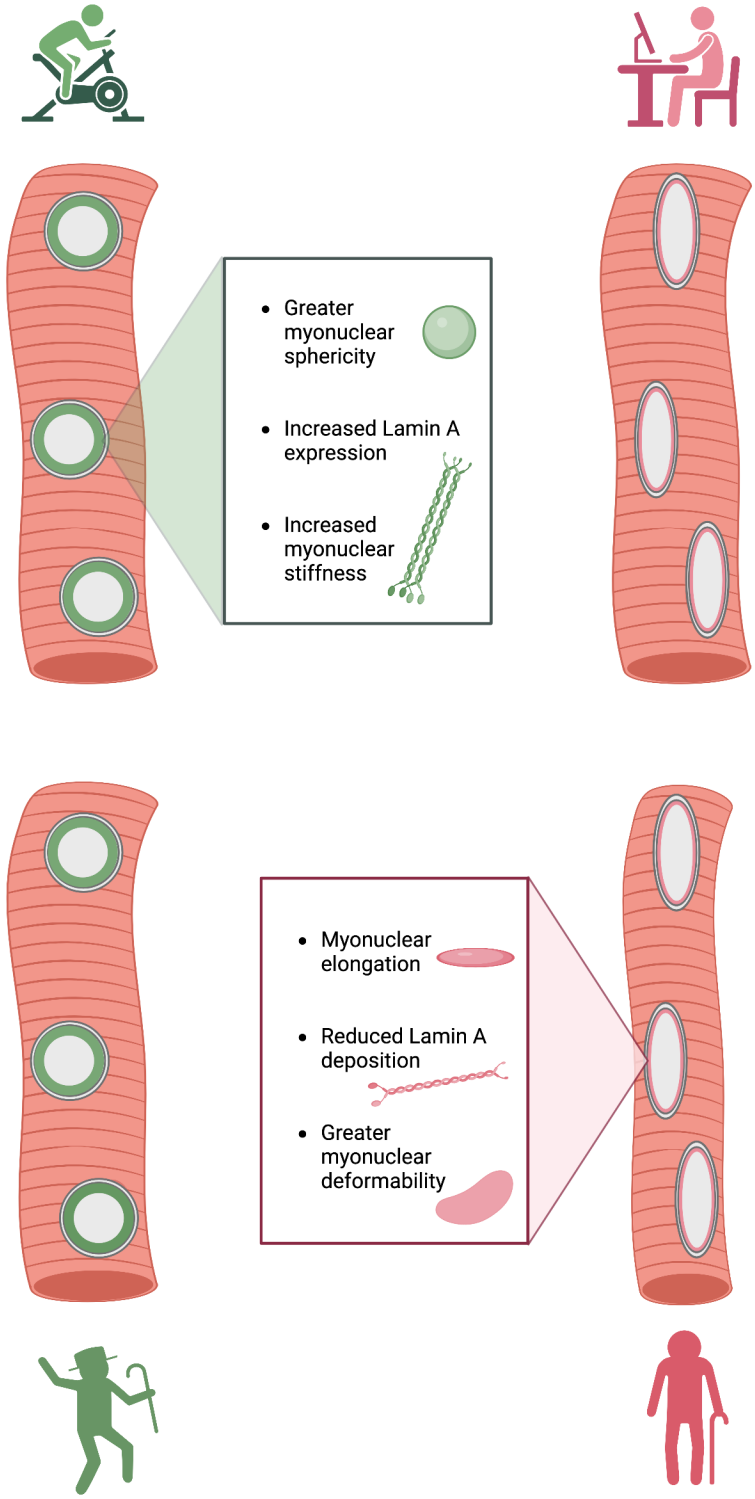

The Journal of Physiology

Abstract figure: Structural and mechanical properties of myonuclei in trained young and aged individuals. In skeletal muscle fibres from trained individuals, myonuclei are more spherical, have greater Lamin A and are stiffer compared to untrained counterparts. This may protect nuclei from damage when subjected to contractile forces during exercise, and permit effective transduction of these forces to regulate gene expression and signalling pathways (mechanotransduction). In skeletal muscle from untrained older individuals, myonuclei are more elongated, nuclear lamina levels are lower, and myonuclei are more deformable. This may increase susceptibility to myonuclear damage and defective mechanotransduction, contributing to declines in muscle mass and function.

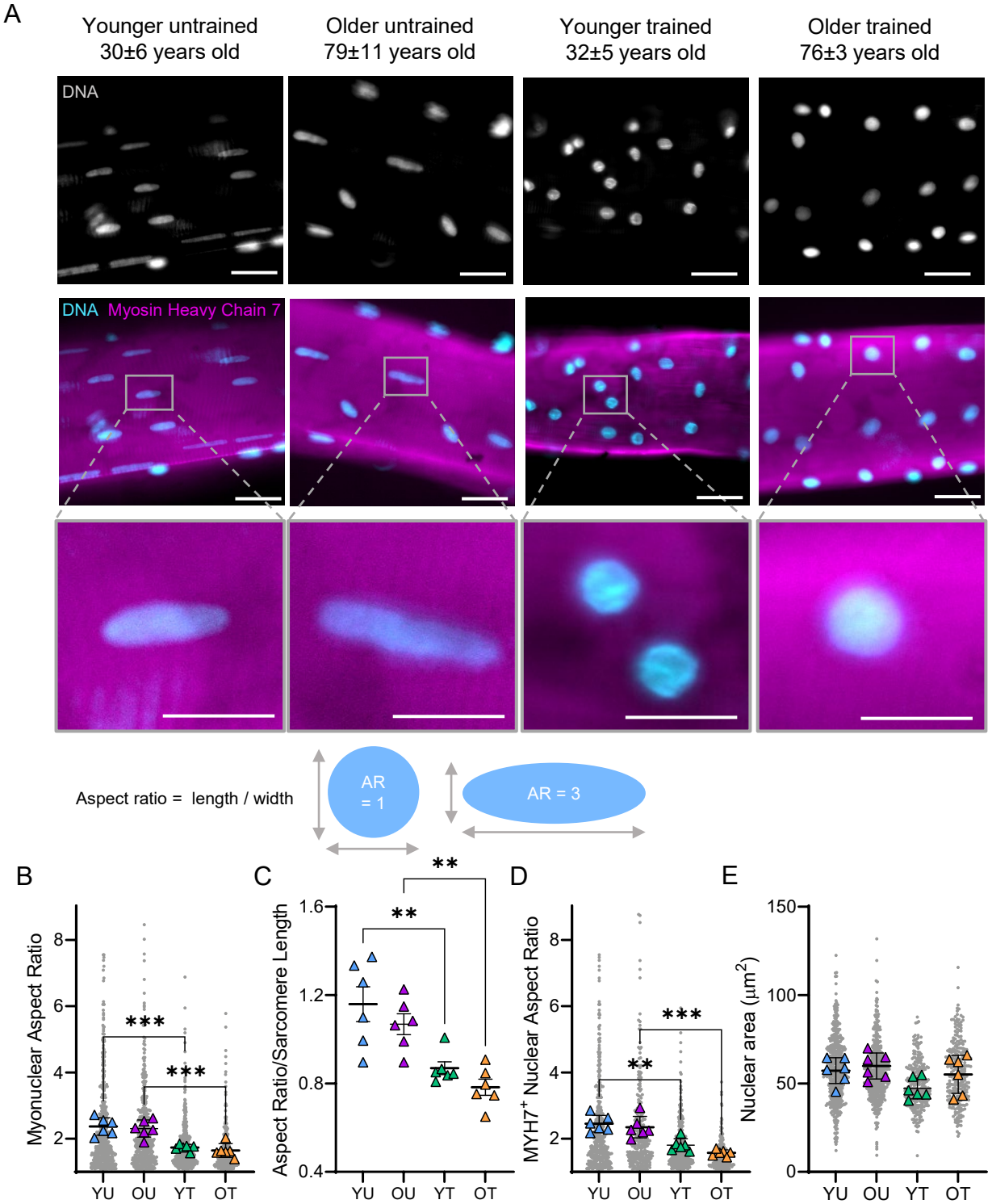

Figure 1. Altered 2D myonuclear shape in trained younger and older individuals (A) Representative images of vastus lateralis muscle fibres isolated from younger untrained (YU), older untrained (OU), younger trained (YT) and older trained (OT) individuals, stained with DAPI (cyan) and Myosin Heavy Chain 7 (magenta) to visualise myonuclei and slow myosin, respectively. Scale bars 30 µm and 10 µm main images and zoomed insets of myonuclei, respectively. (B-E) Calculation of aspect ratio (length/width of nucleus) and nuclear area (µm^2) shown above graphs. (B) Comparisons of myonuclear aspect ratio in YU, OU, YT, and OT individuals; 2053 total nuclei analysed (C) Comparisons of myonuclear aspect ratio between groups after normalisation to sarcomere length (D) Myonuclear aspect ratio in MYH7+ fibres (1385 total nuclei analysed) (E) Comparisons of nuclear area (µm^2) between groups (1453 total nuclei analysed). (B-E) Coloured symbols represent individual means, unfilled grey symbols represent myonuclei; mean values for individuals were used for two-way ANOVA tests (n = 6, ** P < 0.01 *** P < 0.001); error bars represent mean ± SD.

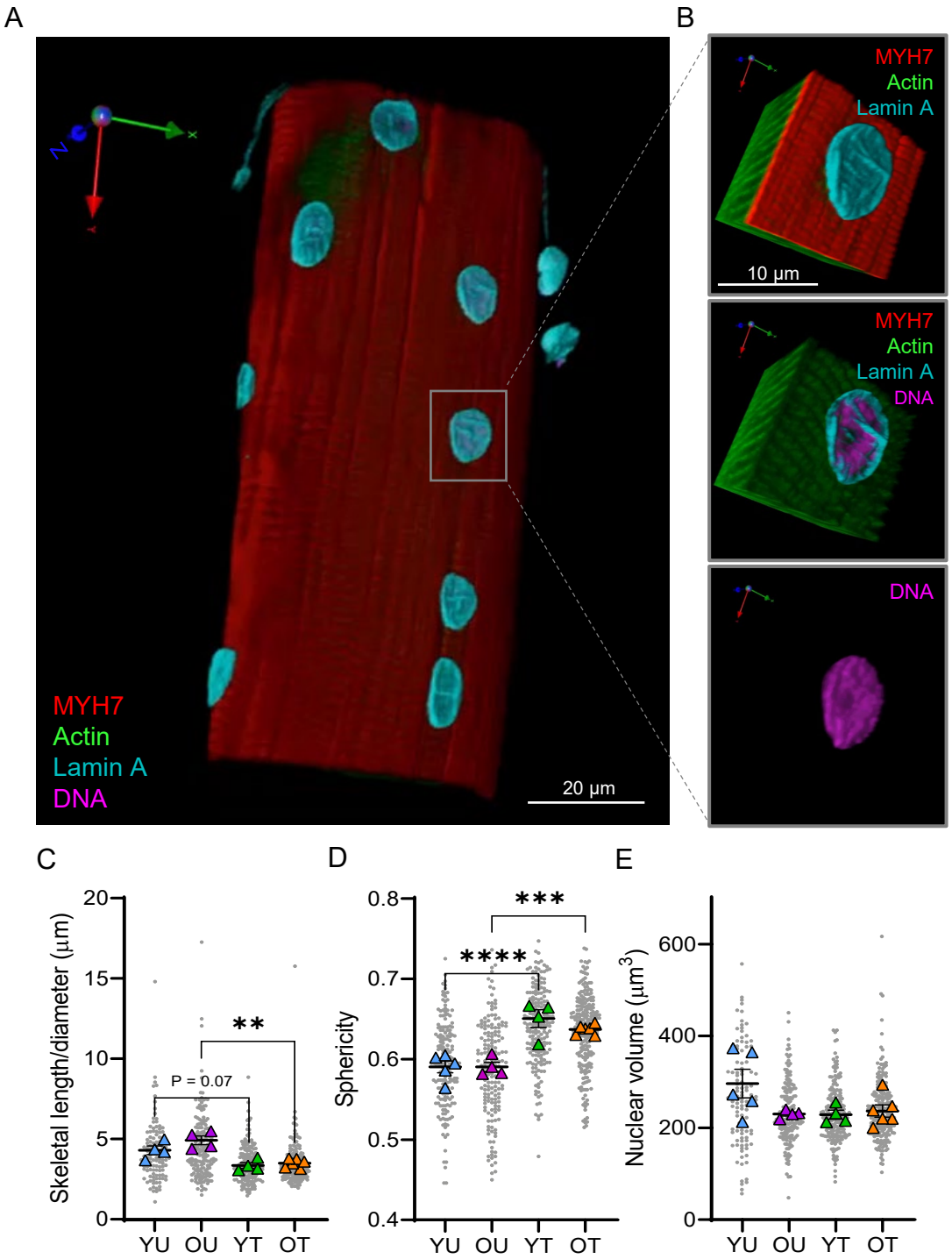

Figure 2. Lower 3D aspect ratio and greater sphericity in myonuclei from trained younger and older individuals (A) Representative three-dimensional rendering of z-stack images of a single human vastus lateralis muscle fibre acquired with a spinning disk confocal microscope equipped with a 63x oil objective lens. Muscle fibre stained to visualise Lamin A (cyan), DNA (magenta), Actin (green), Myosin Heavy Chain 7 (MYH7, red). (B) Representative zoomed images of 3D-rendered nucleus. (C-E) Comparisons of nuclear skeletal length/ diameter (µm), sphericity, and volume in younger untrained (YU), older untrained (OU), younger trained (YT) and older trained (OT) individuals. Coloured symbols represent individual means, unfilled grey symbols represent myonuclei; mean values for individuals were used for two-way ANOVA tests (n = 4-6, ** $P < 0.01$ *** $P < 0.001$ **** $P < 0.0001$); error bars represent mean ± SD.

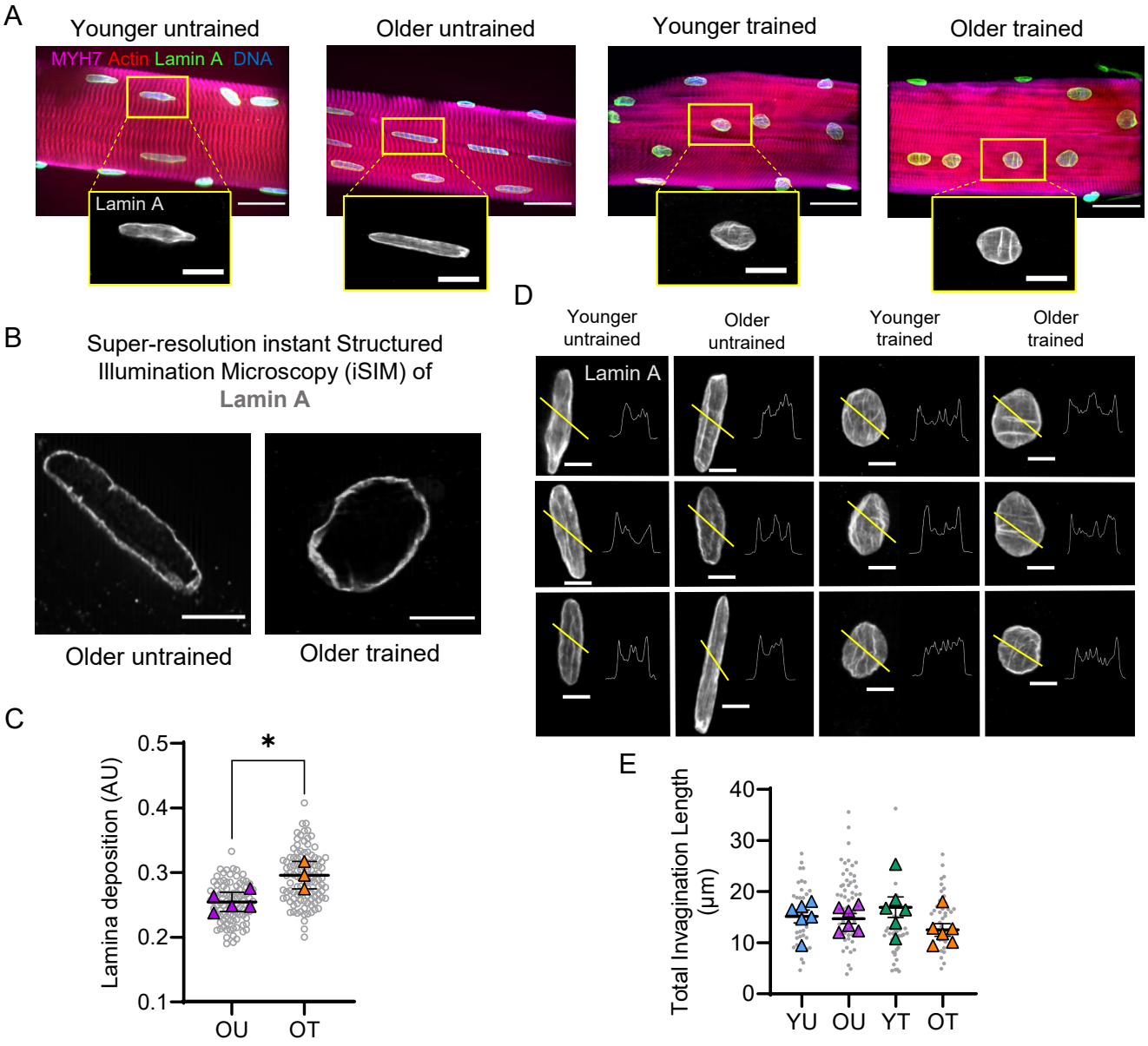

Figure 3: Organisation of Lamin A in trained individuals and untrained counterparts (A) Representative images, acquired through confocal microscopy using a 63x oil objective, of muscle fibres isolated from younger untrained (YU), older untrained (OU) patients, younger trained (YT) and older untrained (OT). Fibres were stained with DAPI to visualise DNA (blue), Actin (red), Lamin A (green, gray) and Myosin Heavy Chain 7 (MYH7, magenta). Scale bar 25 µm in main images, 10 µm in zoomed images. (B) Representative images of myonuclei from OU and OT muscle fibres acquired through super resolution iSIM microscopy. Scale bars 5 µm. (C) Quantification of Lamin A deposition (µm) in muscle fibres from OT and OU. N = 3-5 per group, unpaired t-test revealed significant difference between groups ($P < 0.05$). (D) Standard deviation projections of Lamin A-stained myonuclei and pixel intensity line scans (yellow line) from YU, OU, YT, and OT. (E) Lamin A total invagination length (µm) in muscle fibres from YU, OU, YT, OT, n = 6. Two-way ANOVA revealed no significant differences between groups. Coloured symbols represent individual means, grey symbols represent myonuclei; mean values for individuals were used for two-way ANOVA tests and t-test. Error bars represent mean ± SD.

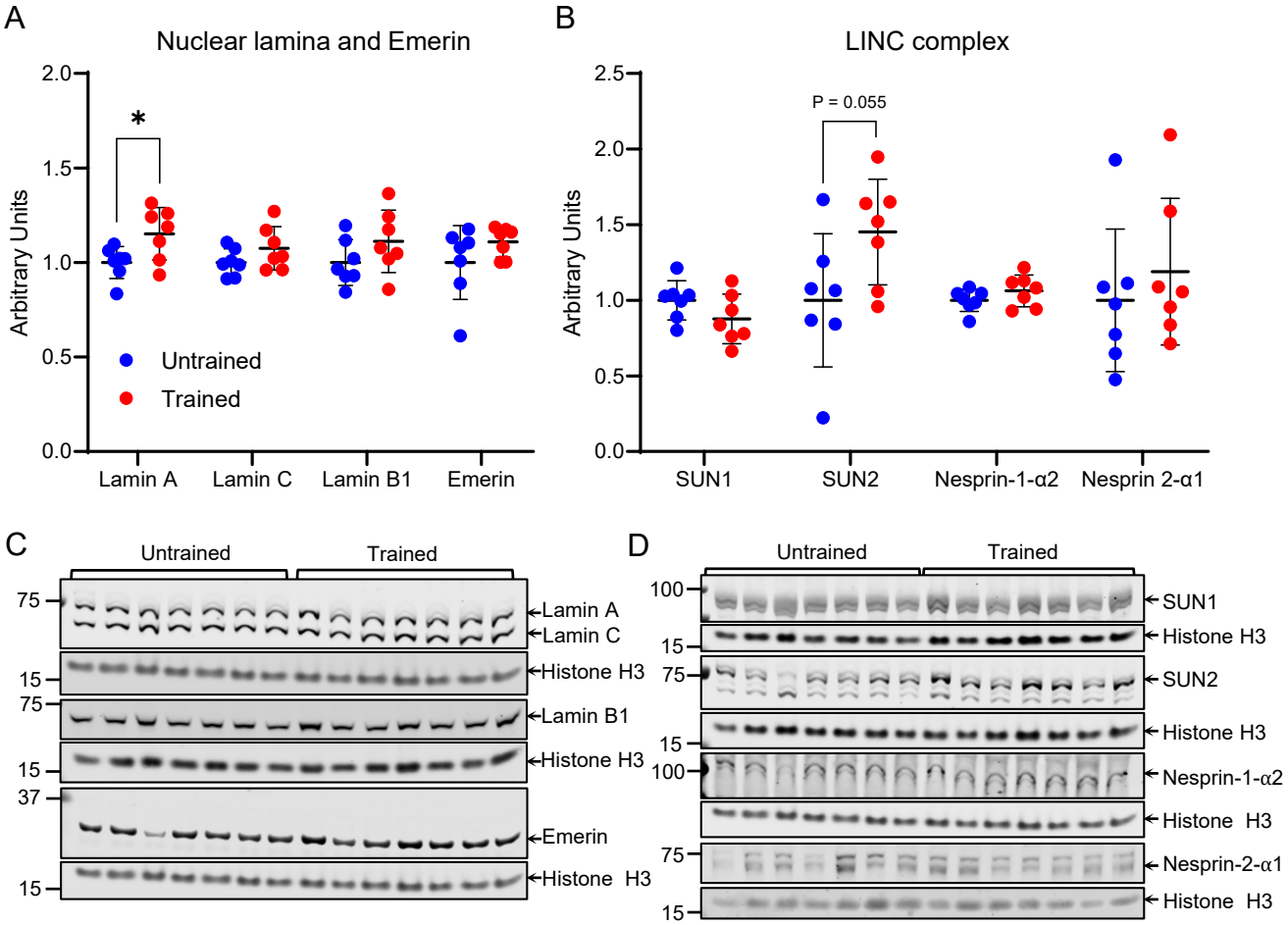

Figure 4: Lamin A levels are increased in trained mouse tibialis anterior muscle (A) Protein levels of Lamin A, Lamin C, Lamin B1 and Emerin normalised to Histone H3 in tibialis anterior muscle from untrained and high intensity endurance trained mice (B) Protein levels of Linker of Nucleoskeleton and Cytoskeleton (LINC) complex proteins SUN1, SUN2, Nesprin-1-α2, and Nesprin-2-α1 normalised to Histone H3 in tibialis anterior muscle from untrained and trained mice (C-D) Images of western blots from which data in A-B were obtained. Note that Lamin A levels were significantly increased and SUN2 levels trending to increase. Arrows indicate predicted molecular weights (kD). Data points represent individual mice, n = 7 per group, * indicates $P < 0.05$ (t-test). Error bars represent mean ± SD.

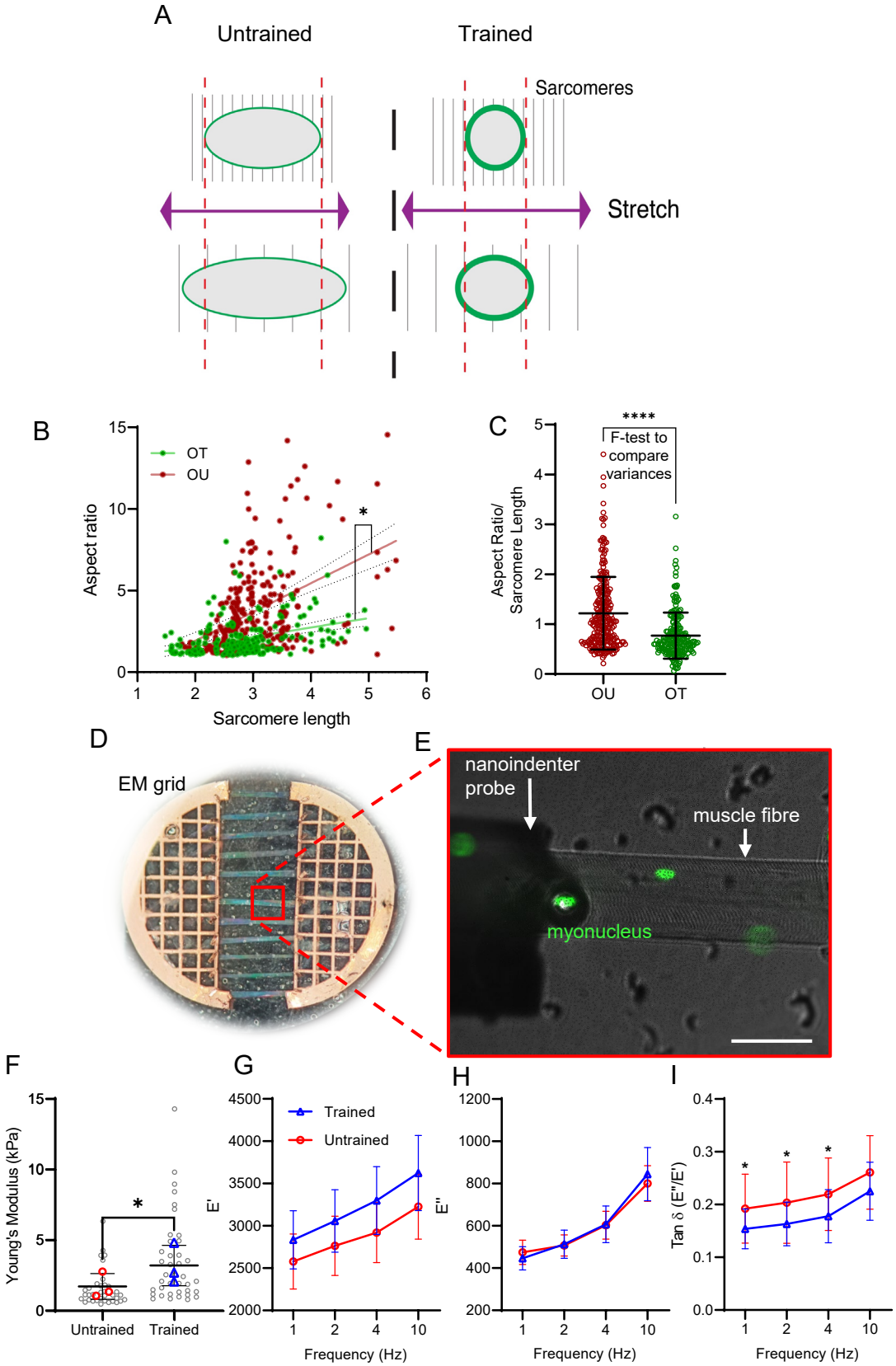

Figure 5. Exercise training results in stiffer myonuclei (A) Schematic of fibre mounting and stretching. (B) Relationship between sarcomere length and nuclear aspect ratio in muscle fibres from older trained (OT) and untrained (OU) patients. (C) Variance of aspect ratio/ sarcomere length in OT and OU fibres. Note that sarcomere length positively correlates with extent of muscle fibre stretch and that myonuclei in OT fibres were significantly stiffer than myonuclei from OU fibres. * denotes statistically significant difference between gradients of slopes (linear regression analysis, F-test to compare variances). (D) Typical setup of individual muscle fibres after isolation and mounting in parallel on an electron microscopy (EM) grid split in half for imaging and nanoindentation. (E) Nanoindentation of single muscle fibres (brightfield) with myonuclei labelled (green) being probed by nanoindenter (brightfield, left of image). Scale bar, 50 µm. (F) Comparison of Young's modulus (kPa) in nuclei from untrained (red) and trained mice (blue) (G-I) comparisons of E', E'' and Tan Delta (E''/E') at different Dynamic Mechanical Analysis (DMA) frequencies (Hz) in nuclei from untrained and exercise trained mice. Note that myonuclei were significantly more stiff and more elastic in fibres from trained vs. untrained mice. Each coloured data point represents the average for each mouse, n = 3 per group. Error bars represent mean ± SEM. * denotes statistically significant difference between groups (t-test and mixed effects analysis).

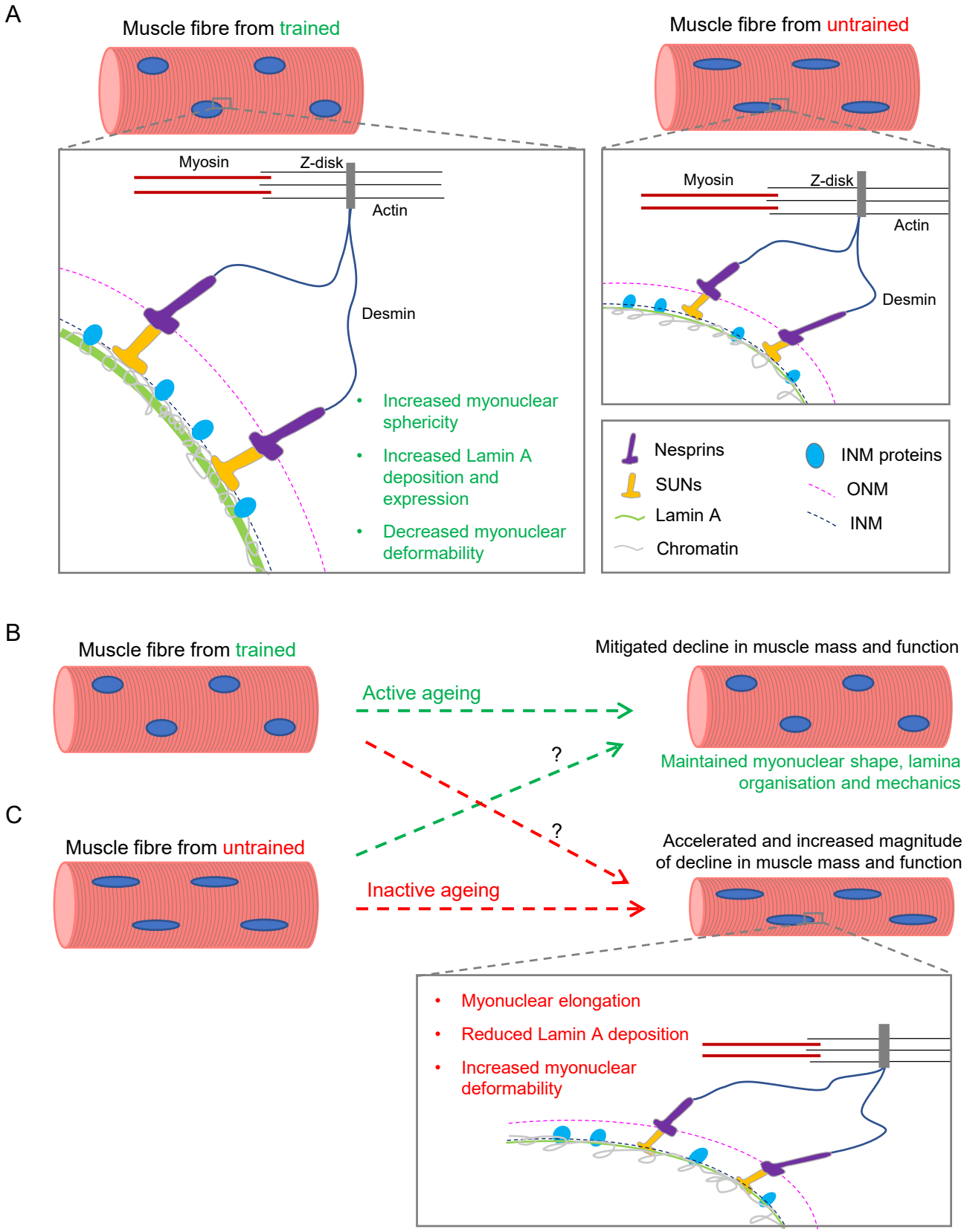

Figure 6. Summary and proposed effects of myonuclear remodelling with training, and inactivity related defects in nuclear mechanotransduction with age (A) In skeletal muscle fibres from trained individuals, nuclear envelope proteins including the nuclear lamina effectively transduce cytoskeletal forces to the nucleus to regulate signalling pathways. (B) In skeletal muscle from trained older individuals, myonuclear shape and mechanotransduction are preserved (C) In skeletal muscle from untrained older individuals, myonuclei are more elongated, nuclear lamina levels are reduced, and myonuclei more deformable. This may lead to increased susceptibility to myonuclear damage and defective mechanotransduction that results in decline in muscle mass and function.